

**Generation of Surface Nanotubes on Titanium Kirschner Wire
for the Enhanced Release of Antibacterial Drug**

BY

LORENZO GIROTTO

B.S. , Politecnico di Milano, Milan, Italy, 2018

THESIS

Submitted as partial fulfillment of the requirements
for the degree of Master of Science in Bioengineering
in the Graduate College of the
University of Illinois at Chicago, 2020

Chicago, Illinois

Defense Committee:

Dr. Markus A. Wimmer, Chair and Advisor

Dr. Mathew T. Mathew

Dr. Roberto Chiesa, Politecnico di Milano

To all Healthcare Workers for COVID-19

ACKNOWLEDGMENTS

I would like to express my deepest gratitude to my advisor, Dr. Markus A. Wimmer, for welcoming me to join the Department of Orthopedics Laboratory and giving me a chance to live an unforgettable experience as well as a priceless opportunity, I will treasure it forever.

Moreover, I am grateful to both other members of the committee, Professor Mathew and Professor Chiesa, for their availability and for taking their time to seal this academic milestone.

I would like to thank all the members of the lab, for sharing with me their invaluable knowledge.

Thank you, Alfons, for all your tips and your engaging stories, you really make research fun.

Thank you, Spencer, for your support and patience, always there for me when I needed you.

Thank you, Simona, for being my Italian colleague and giving me precious game-changing advice.

Thank you, Amandine, I haven't forgotten your promise and I will come get your delicious brioche, eventually.

Thank you, John, for giving me the opportunity to make my humble contribution to your project, I really enjoyed it. Please take care of my mice!

Thank you, Jenna, you really went above and beyond with us, didn't you.

Thank you, Cino, I could not imagine finding a greater colleague and a better friend to steal coffee from.

Thank you, Luco, for being my personal chef and housekeeper. Aueeeeeé

A special thank you to my dad, for correcting this acknowledgment page.

I would also like to thank all my Chicagoan friends, too many to mention here, I spent an incredible year in an amazing city.

Thank you, Chicago, you've been exceptional to me.

TABLE OF CONTENTS

<u>CHAPTER</u>	<u>PAGE</u>
1. INTRODUCTION	1
1.1 Titanium and its Alloys for Medical Implants	1
1.2 Failures of Joint Replacements	2
1.3 Antibiotic Treatment	3
1.4 Surface Modifications Techniques.....	3
1.5 TiO ₂ Nanotubes Formation	4
1.6 Objectives	13
2. MATERIALS & METHODS	14
2.1 Sample Preparation	14
2.2 Electrolyte preparation	15
2.3 Experimental Setup	15
2.4 TiO ₂ Nanotubes Formation	17
2.5 Scanning Electron Microscope (SEM) Evaluation	17
2.6 Raman Spectroscopy	17
2.7 Drug Loading	18
2.8 Drug Release	18
2.9 Reference Vancomycin Solutions for the Calibration Curve.....	19
2.10 UV-Vis Spectroscopy	19

TABLE OF CONTENTS (Continued)

3.	RESULTS AND DISCUSSION.....	22
	3.1 Polishing Evaluation	22
	3.2 TNTs Morphology	23
	3.3 Raman Spectroscopy Evaluation	27
	3.4 Drug Release	29
	3.5 Thickness Analysis	32
4.	Conclusions.....	34
5.	Future Work	35
6.	CITED Literature.....	37
7.	VITA	45

LIST OF TABLES

<u>TABLES</u>	<u>PAGE</u>
TABLE I: DISPOSITION OF COLLECTED SOLUTIONS FROM THE SAMPLES ANALYZED AND 8 REFERENCE SOLUTIONS IN THE 96-WELL PLATE, INCLUDING DPBS ONLY. FROM EACH OF THE 10 WIRES, 6 SOLUTIONS WERE COLLECTED, CORRESPONDING TO THE DIFFERENT TIME STEPS. THE 8 REFERENCE SOLUTIONS WITH KNOWN CONCENTRATION OF VANCOMYCIN WERE INCLUDED 4 TIMES EACH.	21
TABLE II: PARAMETERS USED DURING THE ANODIZATION TO OBTAIN NANOTUBES OF 80 NM DIAMETER.	23
TABLE III: DATA OBTAINED FROM THE MORPHOLOGY OF TNTs.	27

LIST OF FIGURES

<u>FIGURE</u>	<u>PAGE</u>
Figure 1: Electrolytic cell that includes the electrolyte, anode, which in our case is titanium, cathode and power supplier to apply voltage.....	5
Figure 2: Depending on the type of the electrolyte, the native oxide layer of 3-7 nm thickness can grow to form compact TiO ₂ in case of an usual electrolyte (for example containing ammonium pentaborate, ammonium sulfate, or ammonium phosphate [32]), or a nanotubular structure in case the electrolyte contains F ⁻	6
Figure 3: Chemical process of Ti anodization in case of (a) a general electrolyte or (b) in presence of fluoride (F ⁻). F ⁻ allows the formation of the soluble complex [TiF ₆] ²⁻ that dissolves in water creating the nanotubes.....	8
Figure 4: Current density – time curve showing the different behavior of current density within the oxide layer whether the electrolyte contains fluoride (blue) or not (red). In the fluoride-containing electrolyte, the current density shows three distinct phases: (I) the curve follows the fluoride-free case, where the oxide layer thickens as the current density decreases, (II) the current increases due to the initial formation of pores that decrease the resistance of the anodic layer, (III) the process stabilizes as the oxidation rate at the metal-oxide interface equals the dissolution rate at the oxide-electrolyte interface.....	9

LIST OF FIGURES (Continued)

- Figure 5: Effect of the current field on the pore initiation. (A) When the process starts, the current even throughout the whole oxide surface. (B) Due to impurities in the structure of the metal some local variations of the current field take place, causing the growth of oxide in specific spots on the surface. (C) The poor conductivity of the oxide makes the current field lines bend towards areas where the oxide is thinner, causing the formation of nanotubes in specific sites. (D) Once the process is triggered by the defections, the nanotubes keep growing forming a well-defined structure on the surface. 11
- Figure 6: The final diameter of the nanotubes oscillates around an equilibrium point (B) determined by the voltage applied. If the dissolution of oxide is prevalent over the formation of oxide and the diameter increases (A), the current density around the nanotubes increases, causing the nanotube morphology to go back towards the equilibrium point. On the other hand, if the formation of oxide is prevalent over the dissolution and the diameter decreases (C), the current density decreases, causing the nanotube morphology to go back towards the equilibrium point once again. 12
- Figure 7: (a) Setup of the experiment where the Ti wire (anode) is inserted into the cathode of the reaction to form TNTs on the surface; (b) Close-up of the ideal result of TNTs: the small portion of anodized wire is a representation of what the whole surface of titanium should look like..... 13
- Figure 8: K-wire inserted into the tip of the drill press for the polishing procedure 14
- Figure 9: Different steps are shown preparing the experimental setup. (a) shows the beaker filled with electrolyte secured with lab clamps and graphite hollow cylinder fit into the PTFE mask, which is secured with tape at the beaker; in (b) the negative pole is connected to the graphite and secured with lab clamps; (c) shows the final setup, with the positive pole attached to the K-wire, which is inserted in the electrolyte into the graphite.... 16

LIST OF FIGURES (Continued)

- Figure 10: TNTs morphology prior to polishing optimization. Nanotubes did not grow homogeneously on the surface because of many impurities due to a not efficient polishing method. The images were taken at the magnitudes of 10,000x (a) and 20,000x (b).22
- Figure 11: Surface morphology of TNTs seen at the SEM after anodization of Ti at 50 V for 60 min. The figures show a gradual close-up from 5000x magnification (a) to 35,000x (c) with an intermediate 10,000x (b). As seen from (c) the diameter is approximately 80 nm wide and homogeneously distributed on the surface.24
- Figure 12: Surface area comparison between smooth and anodized K-wire considering treatment of 20 mm of wire and assuming the pore length to be about 2 μm . The great increase in surface area is due to the self-organized hollow tubes that are formed on the oxide surface.25
- Figure 13: SEM image of the very tip of the anodized K-wire. It is possible to assume the thickness of the nanotubes layer to be approximately 2 μm , also suggested by other studies [50]–[52] using the same parameters during the process.26
- Figure 14: Gentamicin Raman spectra showing characteristic peaks for gentamicin, a major one at 992 cm^{-1} and a minor one at 790 cm^{-1} , for 3 different concentrations of the antibiotic: 10, 1 and 0.1 mg/ml diluted in DPBS. Considering there is one order of magnitude of difference among the samples, the data show results that are too scattered to consider Raman spectroscopy as a valid method to determine the precise concentration of drug in solution.....28

LIST OF FIGURES (Continued)

- Figure 15: Close-up of gentamicin sample dried on stainless steel substrate taken with 50x objective. Single crystals spread unevenly on the surface making it a discriminating factor for an objective evaluation. The sample taken into consideration had a concentration of 10 µg/ml of gentamicin diluted in DPBS.....29
- Figure 16: Calibration curve obtained from known concentrations of vancomycin diluted in DPBS in order to associate the value of absorbance returned by the UV-Vis spectrometer to the amount of vancomycin released in the solution. The samples chosen were DPBS only, 7.8, 15.63, 31.25, 62.5, 125, 250 and 500 µg/ml of vancomycin in DPBS.31
- Figure 17: vancomycin released from K-wires in 400 µl of DPBS solution after different time steps. The initial burst from TNTs releases twice as much vancomycin in the first minute (blue) compared to smooth titanium (red). The TNTs curve also shows a steeper slope in the following time steps reaching a final release of vancomycin of about 90 µg compared to smooth titanium that releases about 50 µg after 2 hours. .32

LIST OF ABBREVIATIONS

TiO ₂	Titanium Dioxide
THA	Total Hip Arthroplasty
TKA	Total Knee Arthroplasty
PJI	Periprosthetic Joint Infection
TNT	Titania Nanotubes
F ⁻	Fluoride
ELI	Extra Low Interstitial
K-Wire	Kirschner Wire
DI	Deionized
HF	Hydrofluoric Acid
PTFE	Polytetrafluoroethylene
OD	Outer Diameter
ID	Inner Diameter
SEM	Scanning Electron Microscope
DPBS	Dulbecco's Phosphate Buffered Saline
UV-Vis	Ultraviolet-Visible

SUMMARY

Titanium and its alloys are widely used in medical applications for their excellent properties such as biocompatibility, low toxicity, high chemical stability, good fatigue strength, and resistance to corrosion. Unfortunately, those properties do not always prevent the human organism to attack and isolate Ti implants causing explantation and, therefore high costs and inconvenience for the patient. That is why a surface modification is often performed to improve the integration with the tissues without affecting the bulk properties of the material.

Lately, researchers focused their attention on the functionalization of the surface at the nanoscale, which has proven to offer a wide range of applications in many different fields. The goal of this study was to obtain titanium dioxide nanotubes (TNTs) on the surface of titanium implants by anodization. Furthermore, their properties were exploited to load vancomycin in a solution for a drug release test in a potential antibacterial application of the implant in vivo.

The anodization was performed in an ethylene glycol-based solution (98 vol%) containing 0.3 wt% ammonium fluoride (NH_4F) and 2 vol% deionized water. The reaction took place for 60 min at a constant voltage of 50 V with a sweep rate of 1 V/s.

The resulting nanotubes were approximately 80 nm in diameter and hypothetically 2 μm long. The length was solely estimated since we could not obtain cross-sectional images. Compared to a smooth implant, the surface area of the anodized wire increased by 50 times.

Raman spectroscopy did not appear to be a feasible alternative for quantitative analysis of antibiotics in solution. Hence, we opted for ultraviolet-visible (UV-Vis) spectroscopy.

The vancomycin solution was loaded in the implant and a release test was performed. The anodized wires showed to release nearly 80% more antibiotic after 2 hours compared to smooth titanium.

INTRODUCTION

1.1 Titanium and its Alloys for Medical Implants

Titanium and its alloys offer a wide range of applications in the biomedical field due largely to their excellent biocompatibility, low toxicity, high chemical stability, biologically relevant mechanical properties, good fatigue strength, formability, machinability and notable resistance to corrosion [1]–[3]. In particular, the thin layer of titanium oxide (TiO_2) that naturally forms on the surface of titanium endows the material with the previously mentioned attributes which lend themselves to biomedical applications [4]. Repassivation ability and chemical inertness are indeed properties given by the thin layer of titanium oxide, or else called titania, which is typically 3-7 nm thick and found in an amorphous state [5].

Titanium is largely used for bone replacements, artificial joints, and dental implants to restore the original functions of the affected tissue with very good results [2], [5]. Other less common applications are for osteosynthesis implants for bone fracture-fixation, including bone screws, bone plates and maxillofacial implants [2].

Total Hip Arthroplasty (THA) and Total Knee Arthroplasty (TKA), in which implants are made in a great part of titanium and its alloys, represent the most common implants in the United States with 370,000 and 680,000 patients respectively in 2014. This market is bound to grow exponentially in the next years, with a projection of THA reaching 511,000 implants by 2020 and 572,000 by 2030, while TKA is thought to grow at 1.37 million by 2020 and 3.48 million by 2030 [6]. In 2015 it was estimated that at least 7 million of Americans were living with either a hip or knee replacement [7], which amounts to 2% of the population. Moreover, about 60% of orthopedic implants globally include joint replacements and spinal implants [8], where titanium and its alloys are mostly used.

These numbers show how extended the orthopedic implants market is and how important it is to enrich it due to the constant changing demands of orthopedic applications for titanium.

1.2 Failures of Joint Replacements

Unfortunately, a high number of the aforementioned implants does not fully integrate with the patient's body and therefore results in failure. The most common types of failure of orthopedic implants are periprosthetic fracture, dislocation, thrombosis, lack of osseointegration and Periprosthetic Joint Infection (PJI), which typically occurs at early stages after implantation [9], [10]. In particular, the infection can be caused by improper surgical technique or increased exposure during lengthy operations [11]. This leads to the formation of a bacterial derived biofilm that protects bacteria from the immune system, making them 1000 times more resistant to standard antibacterial methods [12]–[14]. PJI not only can cause revision surgery, but also a permanent loss of function, amputation of the limb and, in the worst cases, death [10]. In THA, infection occurs in 0.5-3% in primary implants, which means - in absolute numbers - that at least 2,000 Americans suffer from infection in the hip every year [15], [16]. In TKA, infection occurs in 0.7-2.4% in primary implants [17]–[19], which means that at least 5,000 Americans suffer from infection in the knee every year. Without taking into account the enormous inconvenience for the patient, there is also a high cost for the healthcare system to support, which is supposed to be about \$120,000 for an infected THA and \$90,000 for an infected TKA [20], [21]. These numbers show how important it is to prevent complications in total joint replacements and to find new techniques to guarantee the safety of patients first, but also to avoid a great economic burden to the healthcare system.

1.3 Antibiotic Treatment

Currently, the clinical treatment for biomedical implant infection is the administration of antibiotics that are delivered systemically, but in this case only a very small percentage of the drug is delivered to the site of infection and there can be unwanted off-target interactions. Since it is not possible to increase exponentially the amount of drug administered without toxic consequences, localized delivery of antibiotics at the site of infection or at the implant before the infection is desirable [22]. One possible solution to achieve that is to increase the surface area of the implant incorporating the drug directly on the surface before implantation, thus preventing the drug to circulate in the body where it is not needed. Surface modification and, in particular, the formation of nanotubes on titanium surface is a technique particularly suited for that goal.

1.4 Surface Modifications Techniques

Despite all the good properties owned by titanium, it still does not meet all the requirements to be implanted without negative consequences for the organism. A good method to improve biological, chemical and mechanical properties, without affecting the bulk properties of the material, is to perform a surface modification directly on the implant in order to obtain the desired tunable characteristics.

There are multiple techniques of surface modification to be performed on titanium, including mechanical treatment, thermal spraying, sol-gel, chemical and electrochemical treatment, ion implantation, atomic layer deposition and many others, each of them attributing different properties to the TiO₂ layer [2].

This is the reason why surface modification techniques have caught the interest of many researchers to enhance even more the integration of titanium oxide with the biological environment of interest. It is for these reasons that biomedical research has begun trending towards the study of nanofunctionalization of implants; it has been shown that nanofeatures and

nanoarchitectures are able to innately interact with native tissues and cells because of the biologically relevant size of cells, proteins, and bioactive molecules [23]. Beyond the interaction of engineered nanostructures with native tissues it is also possible to create hybrid compounds integrating biomolecules into the matrix of non-organic biomaterials, such as metals, ceramics or polymers [23].

That is why we decided to focus on the functionalization of nanotubes on titanium surface, which is a promising technique, in order to obtain several benefits: better integration with bone tissue, antimicrobial activity given by the morphology of the treated surface and the possibility to load the surface with biomolecules for a drug delivery application.

1.5 TiO₂ Nanotubes Formation

Previous research has shown that a robust strategy for mitigating the issues discussed in biomedical implants would be the use TiO₂ nanotubes (TNTs) on the surface of titanium implants [24]. TNTs are self-organized structures with great mechanical properties and support fast osseointegration, even more so than the native layer of TiO₂ [25]–[27], and antibacterial properties [14]. The process involves the formation of hollow cylindrical structures on the oxide layer, increasing its thickness, providing a cavity with tunable dimensions that can also host biomolecules, which can range from proteins that improve the osteoconductive capacity to antibiotics to fight a bacterial infection [28]. These features make TNTs a great candidate to be implemented on orthopedic implants.

TNTs are formed by electrochemical anodization, which is an electrolytic passivation process meant to thicken the native layer of oxide on metal surfaces. The elements needed for the anodization are (Figure 1):

- an electrolytic solution,
- the anode, which in our case is represented by titanium,

- the cathode,
- a power supplier that applies voltage to the cell.

The voltage applied makes the current pass through the electrolyte, which triggers the cathode, the negative electrode, to release hydrogen, while at the anode oxygen is released, increasing the thickness of the oxide.

Voltage, time, type of the electrolyte and temperature are tunable parameters that play a major role in the process [29].

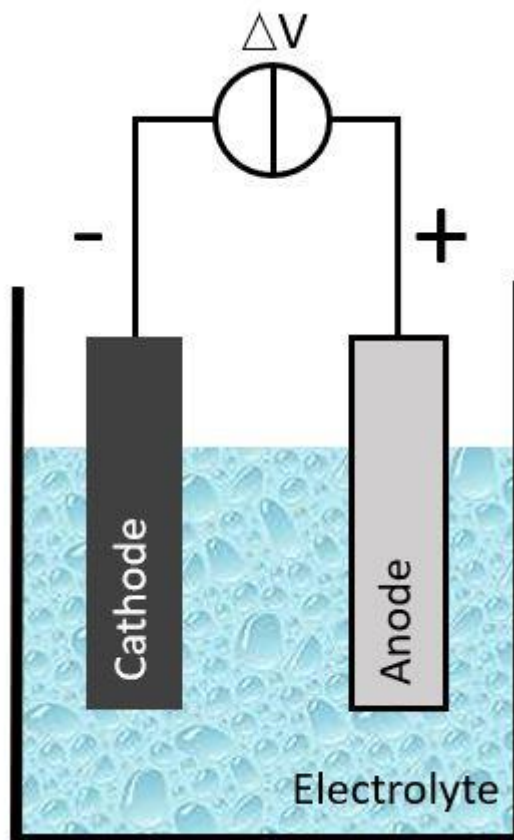


Figure 1: Electrolytic cell that includes the electrolyte, anode, which in our case is titanium, cathode and power supplier to apply voltage.

In the TNTs formation, the presence of fluoride ions (F^-) in the electrolyte strongly affects the process, since they are responsible for the realization of the pores, as seen in Figure 2 [30], [31].

If F^- is not present, the process consists in a controlled growth of oxide resulting in a compact TiO_2 layer.

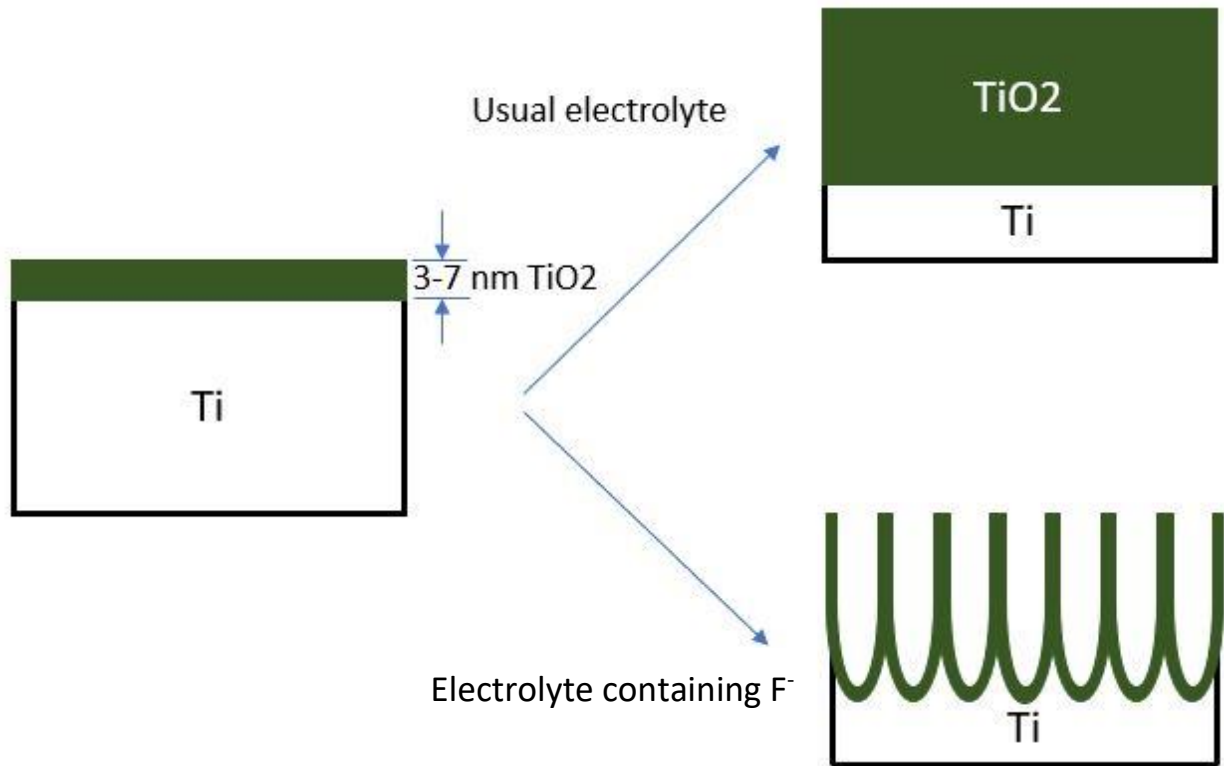


Figure 2: Depending on the type of the electrolyte, the native oxide layer of 3-7 nm thickness can grow to form compact TiO_2 in case of an usual electrolyte (for example containing ammonium pentaborate, ammonium sulfate, or ammonium phosphate [32]), or a nanotubular structure in case the electrolyte contains F^- .

In order to understand the nanotubes formation better, we have to analyze the chemical reactions behind the process. First of all, a thicker oxide layer is formed on the surface, according to Equations (1) – (4):





In the meantime, hydrogen evolution takes place at the cathode of the reaction [Equation (5)]:



Overall, titanium is reacting with H_2O obtaining a growing uniform layer of TiO_2 and gaseous hydrogen [Equation (6)]:



Equations (1) – (6) summarize the oxide formation happening in a fluoride-free electrolyte, where the homogeneous growth is guided by the field-aided transport of ions (O^{2-} and Ti^{4+}) through the oxide layer (Figure 3a).

In presence of fluoride ions, other reactions take place in addition to those previously mentioned. F^- ions have a double effect: they react with Ti^{4+} ions at the oxide-electrolyte interface [Equation 7] and with TiO_2 [Equation 8] forming in both cases water soluble complexes $[\text{TiF}_6]^{2-}$. Figure 3b shows a schematic representation of the process.



The dissolution of those complexes together with the previously described oxide growth of oxide [Equations (1) – (6)], creates a delicate balance in which the formation of nanotubes within the oxide layer is made possible [30], [31], [33].

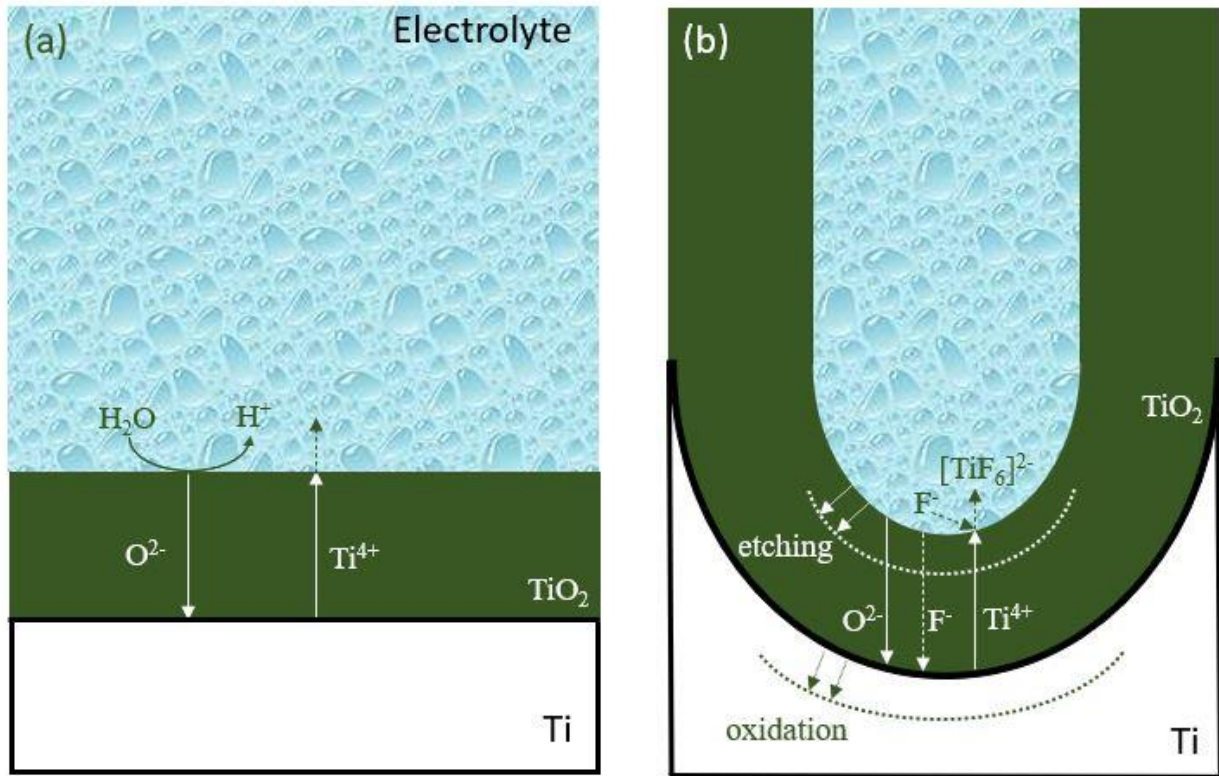


Figure 3: Chemical process of Ti anodization in case of (a) a general electrolyte or (b) in presence of fluoride (F^-). F^- allows the formation of the soluble complex $[TiF_6]^{2-}$ that dissolves in water creating the nanotubes.

The effect of F^- is also evident in the current density – time curve within the oxide layer, shown in Figure 4. Since the reaction is run at a constant voltage (V), in case of a fluoride-free electrolyte, the current field (F) in the oxide decreases as the oxide thickness d increases, until it stabilizes, fixing the thickness. This process is self-limiting as the voltage applied determines the ultimate thickness of the oxide [30], [31], [34]. The current field (F) is determined by Equation (9):

$$F = \frac{V}{d} \quad (9)$$

In the case of an electrolyte containing F^- , the current density within the oxide follows a different path, as seen in Figure 4. Three stages can be observed: (I) The curve follows the fluoride-free trajectory, where we observe the formation of the oxide layer as the current density decreases. (II) The current suddenly increases due to the initial formation of pores that diminish the resistance of

the anodic layer. (III) The current stabilizes as the process reaches a steady-state, that is when the dissolution rate at the oxide-electrolyte interface equals the oxidation rate at the metal-oxide interface [31], [35].

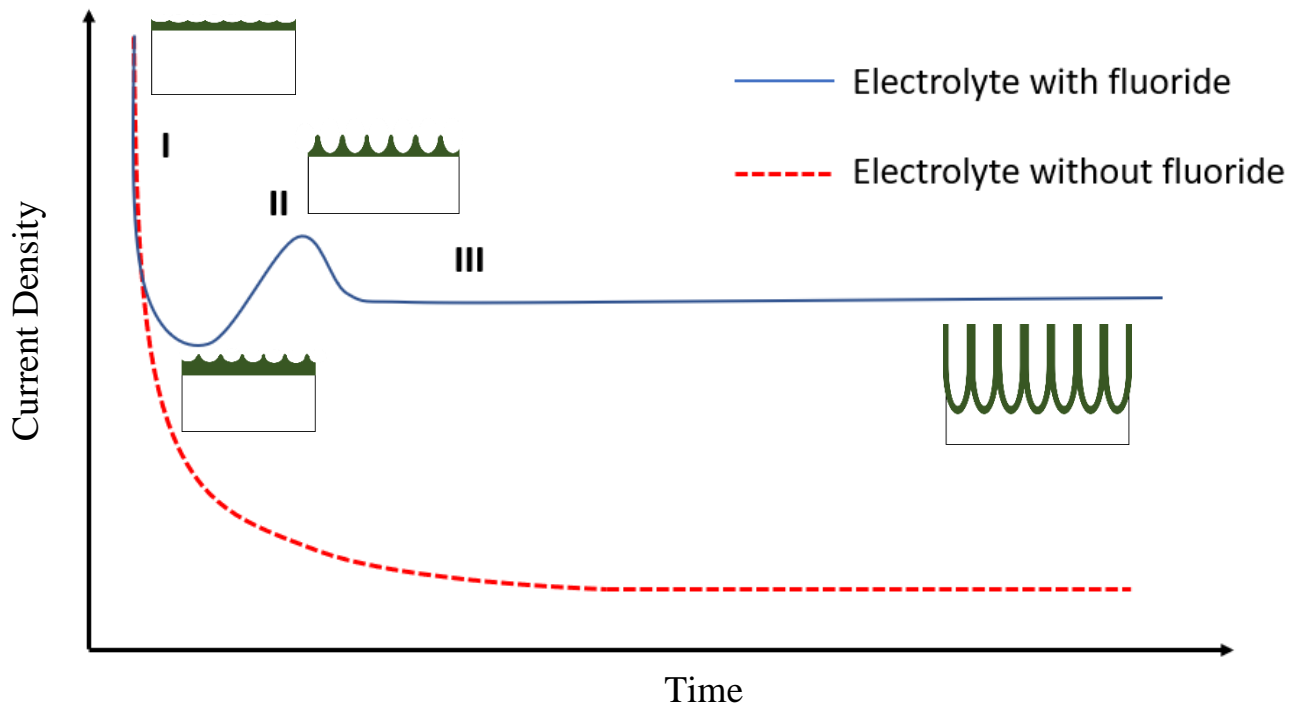


Figure 4: Current density – time curve showing the different behavior of current density within the oxide layer whether the electrolyte contains fluoride (blue) or not (red). In the fluoride-containing electrolyte, the current density shows three distinct phases: (I) the curve follows the fluoride-free case, where the oxide layer thickens as the current density decreases, (II) the current increases due to the initial formation of pores that decrease the resistance of the anodic layer, (III) the process stabilizes as the oxidation rate at the metal-oxide interface equals the dissolution rate at the oxide-electrolyte interface.

The current density plays a major role in the pore initiation and growth, as can be observed in Figure 5 and Figure 6. When the process starts, the current uniformly flows through the titanium oxide layer (Figure 5a). Due to impurities in the structure of the metal some local variations of the current field take place, causing the growth of oxide in specific spots on the surface (Figure 5b). Those defective sites could be the reason for the local growth, making the entry of ions into the film easier. The poor conductivity of the oxide makes the current field lines bend towards areas

where the oxide is thinner, causing the formation of nanoindentations in specific sites (Figure 5c). Once the process is triggered by the defections, the nanotubes keep growing forming a well-defined structure on the surface (Figure 5d) [36]. The mechanism that leads to the pore initiation is not clear yet, however there are two models that hypothesize why the nanotubes growth is related to the impurities in the metal. The two groups of researchers, however, studied alumina nanotubes and not titania ones. The first work by O'Sullivan and Wood [36] suggests that somehow the metal substructure plays a major role, since the pores are formed faster along the boundaries of the metal subgrain. The second model by Macdonald [37] suggests that the initiation of the nanotubes is caused by either the condensation of cations or metal vacancies below the oxide layer. This area is characterized by a high diffusivity of cation vacancies, due to a high disorder in the lattice. The condensation of vacancies leads to a local detachment of the oxide and an interruption of the current flow that initiate the whole growth process.

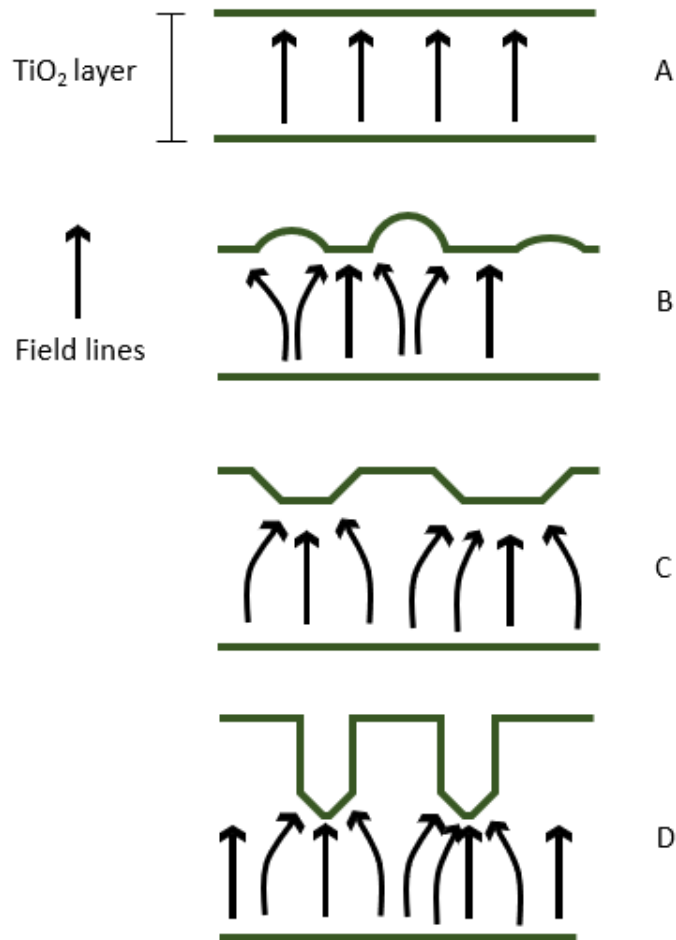


Figure 5: Effect of the current field on the pore initiation. (A) When the process starts, the current even throughout the whole oxide surface. (B) Due to impurities in the structure of the metal some local variations of the current field take place, causing the growth of oxide in specific spots on the surface. (C) The poor conductivity of the oxide makes the current field lines bend towards areas where the oxide is thinner, causing the formation of nanotubes in specific sites. (D) Once the process is triggered by the defects, the nanotubes keep growing forming a well-defined structure on the surface.

Once the nanotubes begin to form, a dynamic process takes place that allow the diameter value to oscillate around an equilibrium point before stabilizing to a fixed value given by the voltage. This process is shown in Figure 6, which depicts the competition between the formation and dissolution of oxide. Since the oxide layer has a poor conductivity, current field lines tend to aggregate where the film is thinner, that is at the base of each nanotube. At the beginning of the formation, which is triggered by impurities in the metal, if the pore happens to be too large considering the voltage

applied (Figure 6a), the current density is low and the oxidation wins over the dissolution, causing the diameter to decrease toward the equilibrium point (Figure 6b). If, on the other hand, the pore happens to be too small (Figure 6c), the high value of current density at the base of the nanotube makes the dissolution to win over the oxidation [38].

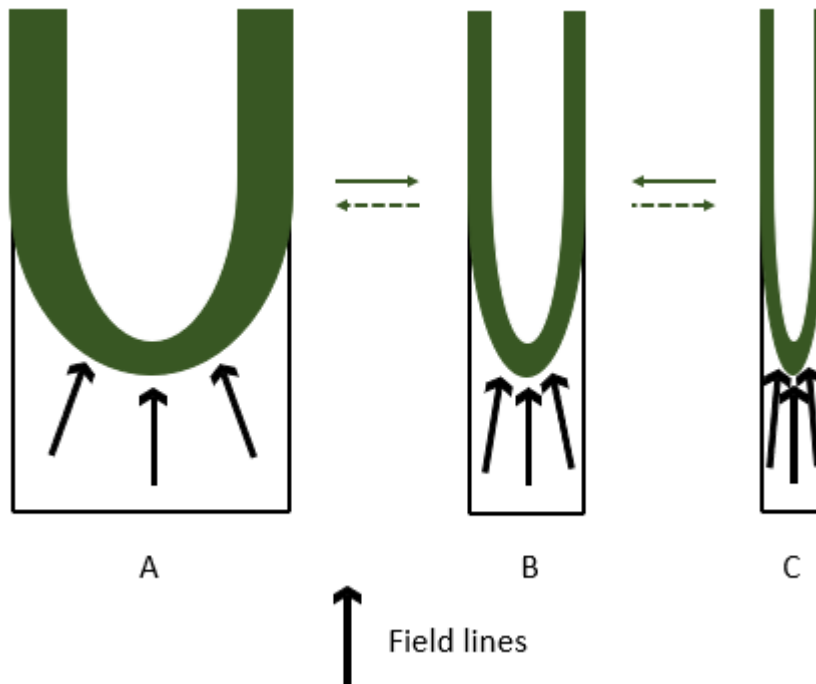


Figure 6: The final diameter of the nanotubes oscillates around an equilibrium point (B) determined by the voltage applied. If the dissolution of oxide is prevalent over the formation of oxide and the diameter increases (A), the current density around the nanotubes increases, causing the nanotube morphology to go back towards the equilibrium point. On the other hand, if the formation of oxide is prevalent over the dissolution and the diameter decreases (C), the current density decreases, causing the nanotube morphology to go back towards the equilibrium point once again.

1.6 Objectives

The goal of this study is to successfully anodize titanium wires to form a homogeneous layer of TNTs on the surface for future in vivo implantation. Figure 7 shows the ideal setup of the experiment and the expected result. The properties of TNTs will also be exploited to load an antibiotic solution to test the ability of the drug release of the nanostructure.

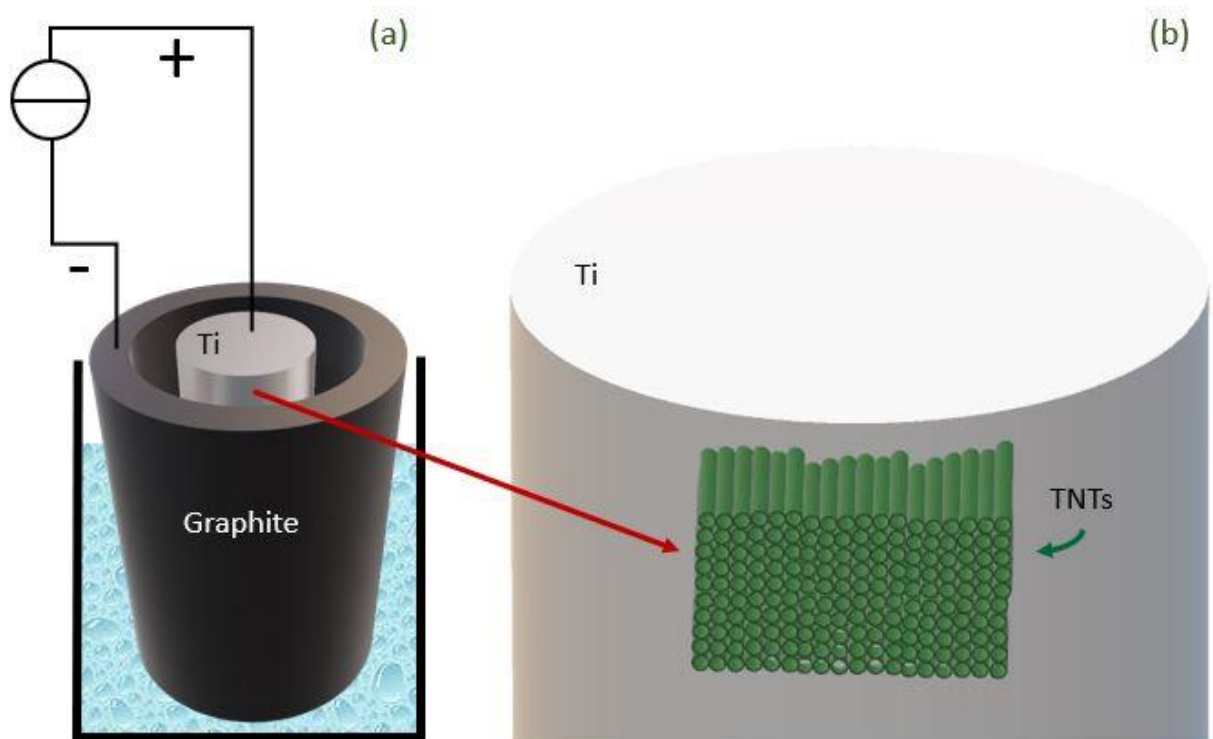


Figure 7: (a) Setup of the experiment where the Ti wire (anode) is inserted into the cathode of the reaction to form TNTs on the surface; (b) Close-up of the ideal result of TNTs: the small portion of anodized wire is a representation of what the whole surface of titanium should look like.

MATERIALS & METHODS

2.1 Sample Preparation

0.6 mm diameter and 30 mm long titanium grade 5 (Ti6Al4V) Extra Low Interstitials (ELI) Kirschner wires (K-wire) were purchased from Custom Wire Technologies, Inc. Before the treatment, the wire was placed into the tip holder of a Pro Tech 10''-12 speed drill press (Figure 8) and mechanically polished while rotating until mirror-like surface was obtained. Different sandpaper grits were used, 320-400-600-800-1200, from rougher to finer grit, as well as 9 μm , 3 μm , 1 μm diamond paste on a cotton disc, in that order. The polishing consisted of swiping for 5 minutes each grit of sandpaper or diamond paste on the rotating titanium rod and removing any debris with a cotton disc sprayed with isopropanol at the end of each step. During the process the sandpapers were kept hydrated with deionized (DI) water in order to reduce the scratches that debris would cause on the surface. The DI water used throughout the whole experiment was purified with Millipore Direct-Q Purification System. The polished K-wire was then sonicated in acetone and methanol for 10 minutes each to remove any dirt, rinsed in DI water and dried in pure nitrogen.



Figure 8: K-wire inserted into the tip of the drill press for the polishing procedure

2.2 Electrolyte preparation

So far, research has seen four generations of electrolytes for the preparation of titania nanotubes [31], [33]. The first generation involves the use of hydrofluoric acid (HF), even if the depth of the tubes can reach no more than 500 nm. The second generation of electrolytes exploits fluoride in solutions containing KF or NaF, but the resulting anodized surface appears rough and not functional. In the third generation, an organic solvent is used, such as ethylene glycol and glycerin. This generation was able to produce very regular structures with well-defined and tunable tube diameters. At last, the fourth generation introduced fluoride-free electrolytes, which can form nanotubes faster, but with less mechanical properties. In fact, it seems they were easily detached from the titanium substrate [39]. It was found by Regonini et al. [35] that the best morphology of nanotubes was obtained with electrolytes from generation three, in particular with ethylene glycol-based solutions with 0.3 wt% of ammonium fluoride (NH_4F) and 2 vol% water.

The electrolyte used was inspired by Wan et al. [40], which belongs to the third generation. It consisted in approximately 120 ml of ethylene glycol-based solution (98 vol%) with 0.3 wt% of ammonium fluoride (NH_4F) and 2 vol% of DI water. The solution was stirred until NH_4F fully dissolved in ethylene glycol and then poured into a cylindrical 120 ml Polytetrafluoroethylene (PTFE) beaker. Glass was not recommended because during the experiment NH_4F might react with water to form hydrofluoric acid (HF) [41].

2.3 Experimental Setup

The voltage for the reaction was provided by DELTA ELEKTRONIKA BV SM700 – series 600/700 watts power supply that contacted the positive pole to the K-wire (anode) and the negative pole to a hollow graphite cylinder, which acted as the cathode of the reaction. The graphite cylinder was manually sawed to obtain approximately a 40 mm long stick and longitudinally drilled to form a hole of 8 mm inner diameter (ID) out of the initial 13 mm outer diameter (OD) to host the

titanium rod during the reaction. The electrolytic cell was composed by the PTFE beaker, where the ethylene glycol-based solution previously described was poured, and a PTFE mask specifically created for holding the graphite cylinder. The mask was manually drilled at the center to create a 13 mm hole so the graphite cylinder could perfectly fit and suspend into the electrolyte. The beaker and the alligator clips were secured with lab clamps to prevent any sort of movement during the experiment. The reaction took place under a ventilated hood. Figure 9 shows a picture of the experimental setup, also shown as a diagram in Figure 7a.

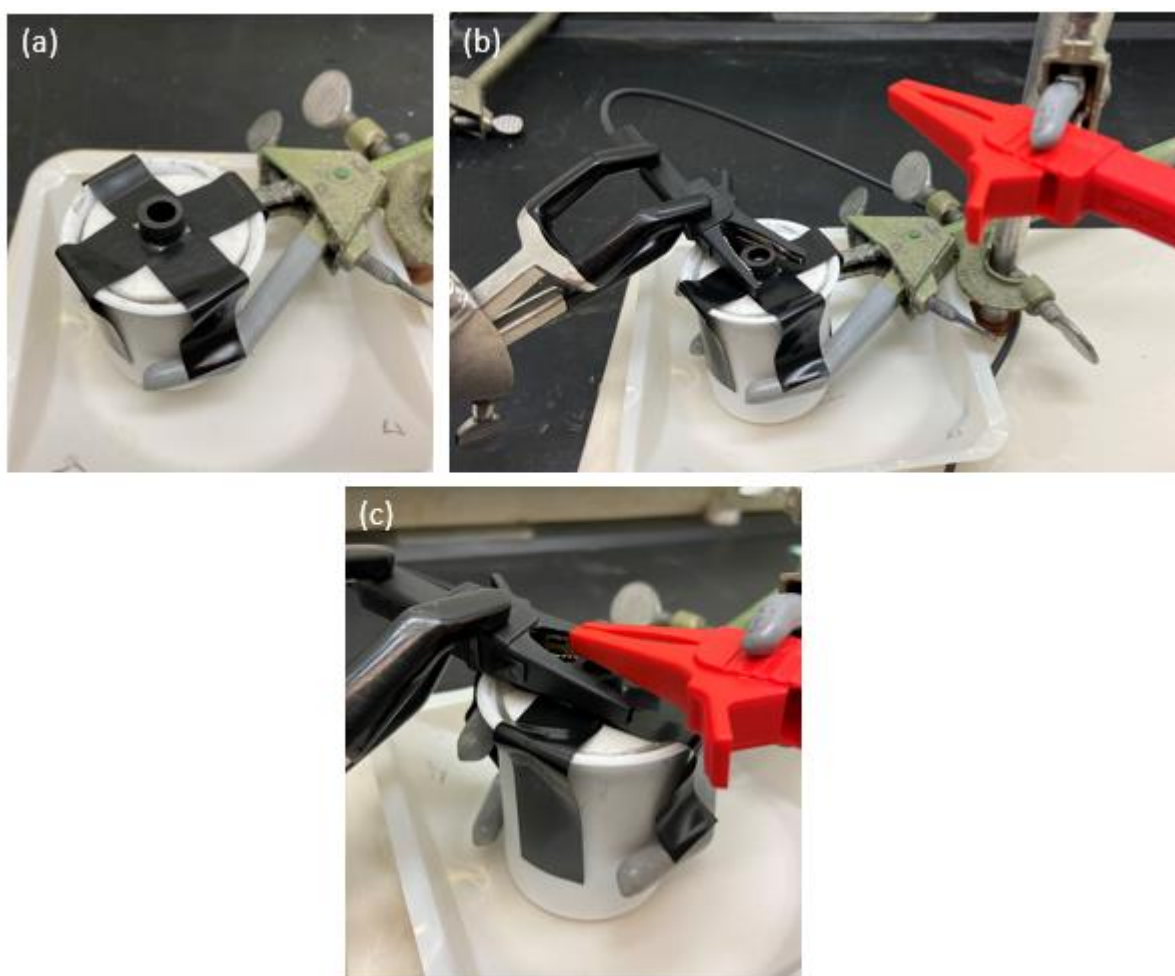


Figure 9: Different steps are shown preparing the experimental setup. (a) shows the beaker filled with electrolyte secured with lab clamps and graphite hollow cylinder fit into the PTFE mask, which is secured with tape at the beaker; in (b) the negative pole is connected to the graphite and secured with lab clamps; (c) shows the final setup, with the positive pole attached to the K-wire, which is inserted in the electrolyte into the graphite.

2.4 TiO₂ Nanotubes Formation

The polished K-wire was contacted to the positive pole of the power supply and gently placed in the electrolyte in the middle of the hollow graphite cylinder, at a distance of approximately 4 mm from the graphite inner wall. The power supply was turned on and the voltage was taken to 50 V with a sweep rate of 1 V/s to prevent a violent reaction. The anodization took place at constant voltage for 60 min. At the end the titanium rod was taken out of the electrolyte, rinsed with DI water and dried in nitrogen. The treated wire was then kept into small plastic bags before further evaluation.

2.5 Scanning Electron Microscope (SEM) Evaluation

The morphology of titania nanotubes was evaluated with Jeol JSM-IT500HR InTouchScope Scanning Electron Microscope (SEM). The samples were gold-sputtered before the observation with Cressington Carbon Coater 108carbon/A. This was necessary to improve the conductivity of the sample surface since TiO₂ alone is not conductive and otherwise, the SEM observation would not be feasible. The acceleration voltage used during the reading was 20 kV and the pictures were taken at magnitude ranging from 1000x to 50,000x. Multiple scans were performed along the rod to confirm the presence of nanotubes on the entire treated surface.

2.6 Raman Spectroscopy

Raman spectroscopy (Horiba LabRAM HR Evolution) was used in a preliminary study with gentamicin (Sigma Aldrich) to verify whether the antibiotic spectra had a specific peak and to distinguish the different concentrations in solution. 10 mg of gentamicin powder were weighed on the analytical balance AX205 DeltaRange Mettler Toledo and dissolved in 1 ml of Dulbecco's Phosphate-Buffered Saline (DPBS) (Gibco) obtaining a concentration of 10 mg/ml, which is reported to be the maximum solubility of gentamicin in DPBS [42]. 500 μ l were taken from the

solution and diluted with 500 μl of fresh DPBS obtaining 1 ml solution at 5 mg/ml. This dilution process was repeated until four concentrations at different order of magnitude were obtained, which are 10 mg/ml, 1 mg/ml, 0.1 mg/ml and 0.01 mg/ml. One droplet of 15 μl from each concentration was pipetted on a stainless steel substrate, which is not Raman active and does not show background signals in the spectra, and the measurements were made with objectives 10x and 100x and Duoscan camera in order to cover a wider area of the substrate.

2.7 Drug Loading

Ultimately, vancomycin hydrochloride from *Streptomyces orientalis* (Sigma Aldrich) was chosen as the loading antibiotic since it is reported to be the most effective against *Staphylococcus aureus* [43]–[45], which is the bacteria used in further studies. After the anodization process the titanium wire was gently rinsed with DI water, dried in nitrogen and let dry for at least 30 min under hood to remove any remaining electrolyte in the nanopores. In the meantime, 400 μl of DPBS were prepared and 40 mg of vancomycin were dissolved in it to make a 100 mg/ml solution. After 30 min the rod was immersed in the 400 μl solution for 10 min and gently shaken to allow the antibiotic in solution to be loaded into the nanotubes. The wire was then removed from the solution and dried for 30 min under hood. This loading/drying process was repeated 3 times to increase the amount of vancomycin in the nanotubes.

2.8 Drug Release

A 500 μl Eppendorf tube was previously filled with 400 μl DPBS to host the loaded rod. The K-wire was then dipped into the Eppendorf tube so that the vancomycin could be released in solution. At different time steps (1 – 5 – 10 – 30 – 60 – 120 min) 300 μl out of the original 400 μl were collected with an Eppendorf Research pipette and placed in different wells in a 96-well plate. Right after the collection of solution at each time step, an equal volume of fresh DPBS was pipetted

into the Eppendorf tube to restore the original 400 μl . The collection of samples and the introduction of fresh DPBS in the solution to restore the original balance were taken in consideration for the following measurements. The final result was 6 wells filled with 300 μl of solution, one for each time step. This proportion (300 μl collected out of 400 μl) was thought to obtain the maximum concentration of vancomycin in the 300 μl sample since the maximum capacity of the well is 300 μl and the sensitivity of the UV-Vis spectrophotometer is directly proportional to the volume of the sample.

In the experiment, 10 K-wires were tested, 5 of them were anodized and dipped in vancomycin solution, while the other 5 were only mechanically polished and dipped in the same solution for the same amount of time.

2.9 Reference Vancomycin Solutions for the Calibration Curve

In order to link the amount of vancomycin in the released solution and the value of absorbance returned by the UV-Vis spectroscopy, different vancomycin solutions were prepared with known concentration of the antibiotic for the purpose of building a calibration curve. 5 mg of vancomycin were first weighed on the analytical balance AX205 DeltaRange Mettler Toledo and diluted in 5 ml of DPBS obtaining a 1 mg/ml vancomycin solution. 8 reference samples of 2 ml volume each were then prepared, starting from 500 $\mu\text{g}/\text{ml}$ to 7.8 $\mu\text{g}/\text{ml}$ of vancomycin in DPBS, halving each time the concentration, obtaining 500, 250, 125, 62.5, 31.3, 15.6, 7.8 $\mu\text{g}/\text{ml}$ solutions. The 8th reference sample was DPBS only.

2.10 UV-Vis Spectroscopy

UV-Vis spectroscopy is a method to quantify different analytes in a solution using light in the UV and visible range. Light excites bonding and non-bonding electrons present in the molecular orbitals and depending on the light's wavelength, different analytes absorb it in different ways,

directly proportional to their concentration [46]. The amount of vancomycin released was determined by measuring the absorbance of light of each sample with a plate reader Perkin Elmer 1420 Multilabel Counter Victor 3 V. Each well of the 96-well reader was filled with 6 collected samples from the Eppendorf tube containing the loaded K-wire, corresponding to the 6 different time steps, and the 8 reference samples with a known concentration of vancomycin. Each reference sample was included 4 times to minimize potential errors. A sketch of the 96-well plate is shown in TABLE I. This method was adopted to avoid systematic errors that would have been caused by measuring in different plates the samples and the references. In this way, we did not account for absolute values of absorbance, but only for the relative difference between the absorbance of the reference and the samples. The wavelength of the light beam was chosen to be 280 nm (UV region), as it is reported to be the maximum absorption of vancomycin [47], [48]. Prior to the reading, the plate was shaken with an orbital movement to have more homogeneous samples and 3 consecutive measurements were made and averaged.

TABLE I: DISPOSITION OF COLLECTED SOLUTIONS FROM THE SAMPLES ANALYZED AND 8 REFERENCE SOLUTIONS IN THE 96-WELL PLATE, INCLUDING DPBS ONLY. FROM EACH OF THE 10 WIRES, 6 SOLUTIONS WERE COLLECTED, CORRESPONDING TO THE DIFFERENT TIME STEPS. THE 8 REFERENCE SOLUTIONS WITH KNOWN CONCENTRATION OF VANCOMYCIN WERE INCLUDED 4 TIMES EACH.

1.1	1.2	1.3	1.4	1.5	1.6	9.1	9.2	9.3	9.4	9.5	9.6
2.1	2.2	2.3	2.4	2.5	2.6	10.1	10.2	10.3	10.4	10.5	10.6
3.1	3.2	3.3	3.4	3.5	3.6	Ref1.1	Ref2.1	Ref3.1	Ref4.1	Ref5.1	Ref6.1
4.1	4.2	4.3	4.4	4.5	4.6	Ref7.1	DPBS1	Ref1.2	Ref2.2	Ref3.2	Ref4.2
5.1	5.2	5.3	5.4	5.5	5.6	Ref5.2	Ref6.2	Ref7.2	DPBS2	Ref1.3	Ref2.3
6.1	6.2	6.3	6.4	6.5	6.6	Ref3.3	Ref4.3	Ref5.3	Ref6.3	Ref7.3	DPBS3
7.1	7.2	7.3	7.4	7.5	7.6	Ref1.4	Ref2.4	Ref3.4	Ref4.4	Ref5.4	Ref6.4
8.1	8.2	8.3	8.4	8.5	8.6	Ref7.4	DPBS4				

RESULTS AND DISCUSSION

3.1 Polishing Evaluation

Different polishing techniques were experimented in order to obtain a mirror-like surface prior the anodization, all of them included just a mechanical polishing of the wire with different grits of sandpaper and diamond paste. Polishing allows to obtain shiny and smooth surfaces which are necessary for the nanotubes to grow perpendicularly and homogeneously on the surface. Figure 10 clearly shows how important the polishing step before the electrochemical process is. In the case shown in Figure 10, the polishing process had not thoroughly treated the whole surface, leaving irregular spots that grew together with the nanotubes. This resulted in uneven dimensions of the pores, cracks distributed on the surface and oxide layers covering the top of the nanotubes. The solution to this problem was to develop an original polishing procedure which is well described in paragraph 2.1.

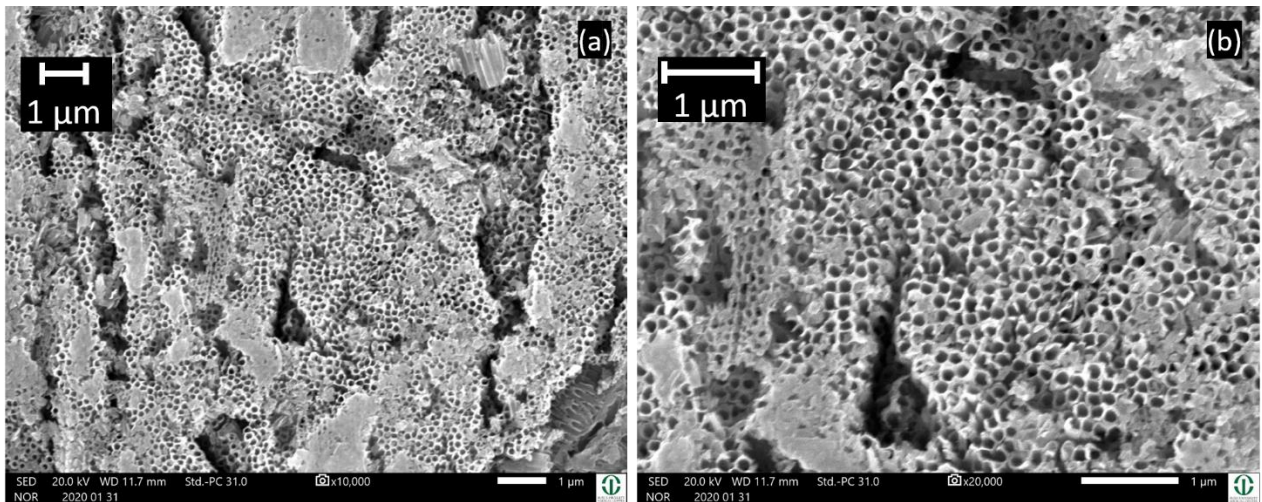


Figure 10: TNTs morphology prior to polishing optimization. Nanotubes did not grow homogeneously on the surface because of many impurities due to a not efficient polishing method. The images were taken at the magnitudes of 10,000x (a) and 20,000x (b).

3.2 TNTs Morphology

The anodization of titanium K-wires resulted in nanotubes with a diameter of approximately 80 nm, which were obtained at 50 V for 60 min with a voltage sweep of 1 V/s. Images of the surface morphology of treated wires were taken at the SEM (Figure 11) with different magnitudes: 5000x, 10,000x, 35,000x. A clear view of the nanotubes can be seen from Figure 11c, while from Figure 11a, it is evident how the reaction took place all over the surface, forming a homogeneous layer of pores, solving the polishing issue completely. The parameters used during the anodization are summarized in TABLE II.

TABLE II: PARAMETERS USED DURING THE ANODIZATION TO OBTAIN NANOTUBES OF 80 NM DIAMETER.

Electrolyte	Voltage	Time	Temperature	Sweep rate
0.3 wt% NH ₄ F + 2 vol% H ₂ O in ethylene glycol [40]	50 V	60 min	20°C	1 V/s

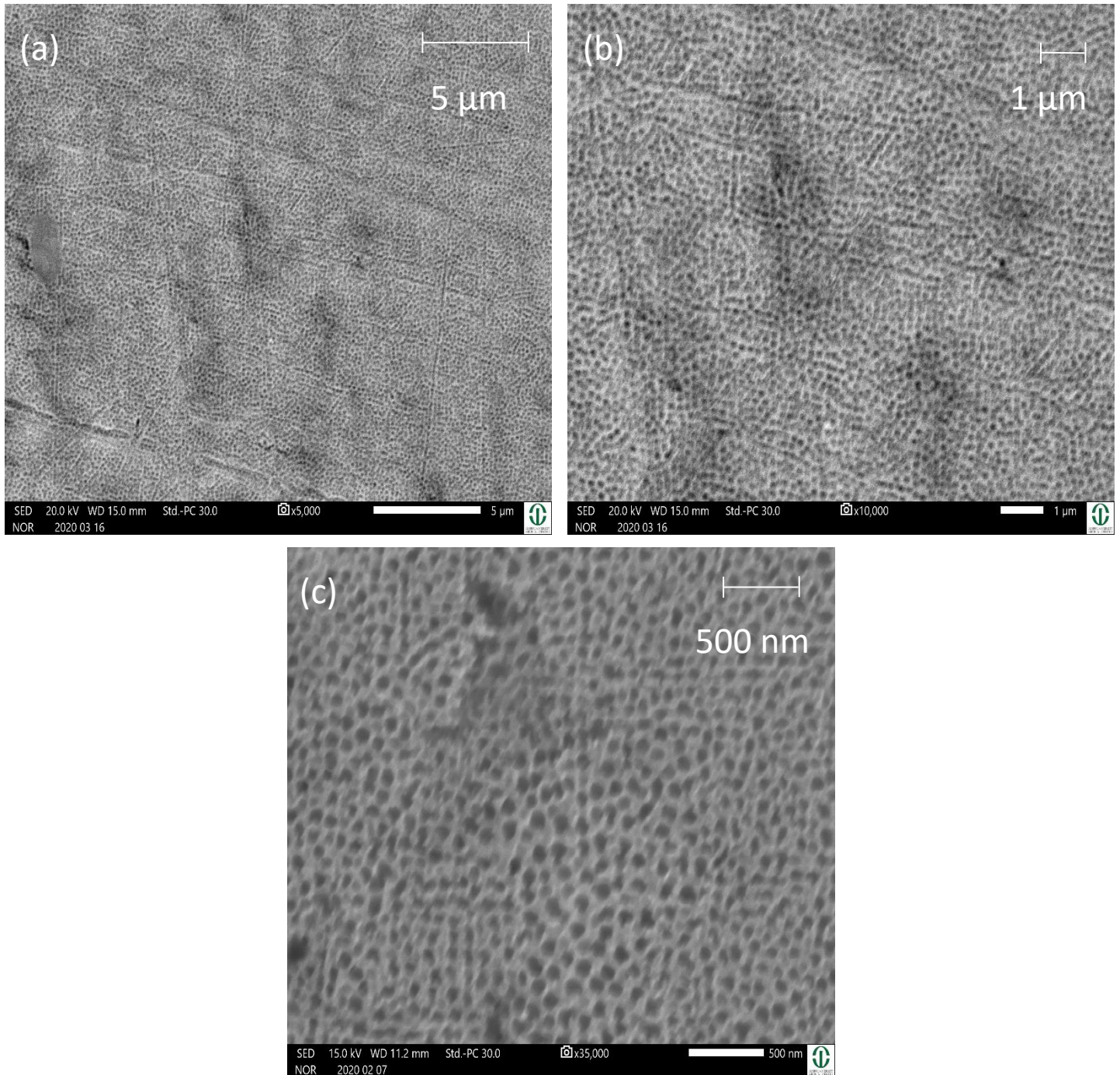


Figure 11: Surface morphology of TNTs seen at the SEM after anodization of Ti at 50 V for 60 min. The figures show a gradual close-up from 5000x magnification (a) to 35,000x (c) with an intermediate 10,000x (b). As seen from (c) the diameter is approximately 80 nm wide and homogeneously distributed on the surface.

The great advantage of forming nanotubes on metal surfaces is the much higher surface area obtained after the process. The hollow nanostructure increases the surface area exponentially, allowing biomolecules to adsorb in great amount into the nanopores, in order to be released over time with greater efficacy.

The formation of 80 nm diameter nanotubes on the surface brings several benefits: it is reported to be the best dimension to achieve the highest antibacterial effect against *S.aureus* [14], [49]. Furthermore, it provides a substrate for the fastest adhesion and proliferation of cells [14], [50] and it increases the surface area, as was previously mentioned, for a potential application of drug loading. With the obtained configuration, 20 mm of K-wire were anodized, which brought an increase in the surface area of 50 times compared to smooth titanium as seen in Figure 12. The measurement was done considering an average tube diameter of 80 nm, a length of 2 μm and a density of 100 tubes/ μm^2 . The great increase in surface area is due to the self-organized hollow tubes that are formed on the oxide surface.

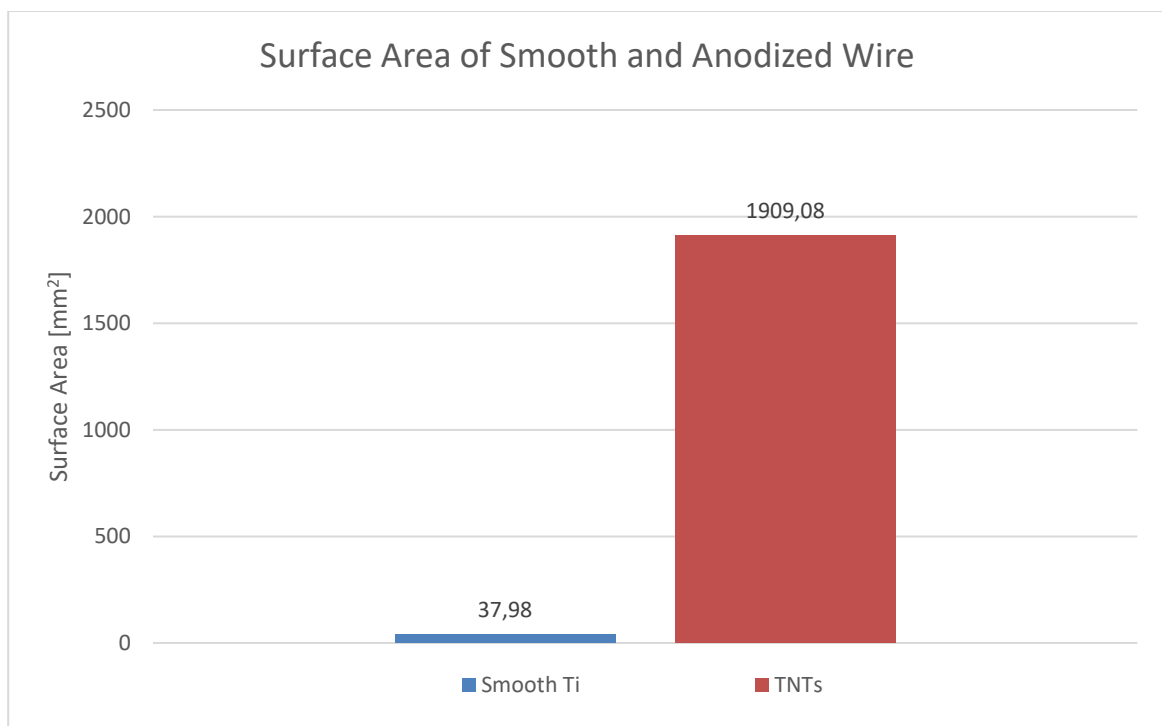


Figure 12: Surface area comparison between smooth and anodized K-wire considering treatment of 20 mm of wire and assuming the pore length to be about 2 μm . The great increase in surface area is due to the self-organized hollow tubes that are formed on the oxide surface.

Unfortunately, cross-section images could not be taken with the SEM; therefore, the thickness of the nanotubes layer could not be evaluated. It was then assumed to be 2 μm considering the type of electrolyte, the parameters used during the anodization and the information found in the literature [50]–[52]. The only proof used to confirm our assumption was a picture taken at the SEM of the very tip of the K-wire, shown in Figure 13, where it is possible to observe a probable thickness of 2 μm .

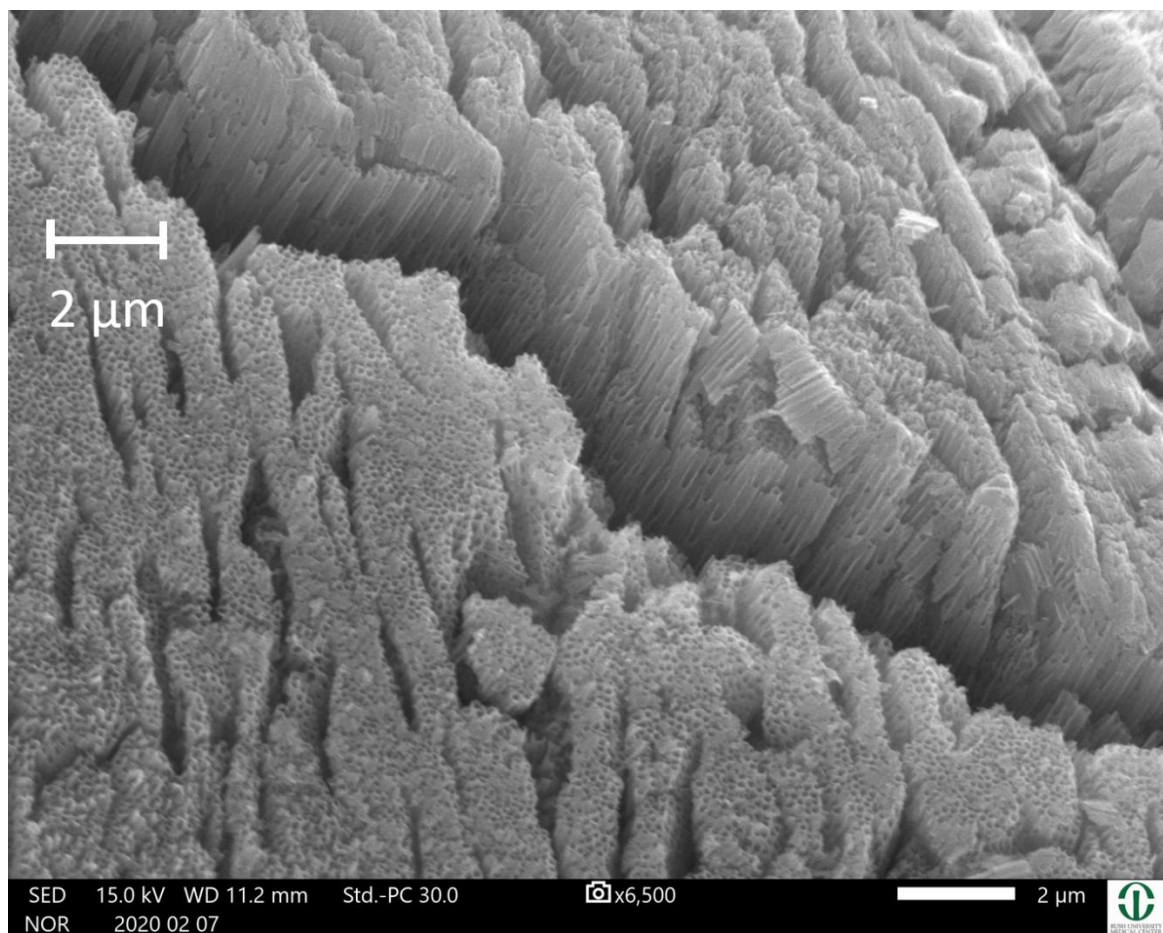


Figure 13: SEM image of the very tip of the anodized K-wire. It is possible to assume the thickness of the nanotubes layer to be approximately 2 μm , also suggested by other studies [50]–[52] using the same parameters during the process.

The information obtained from the morphology of TNTs can be summarized in TABLE III.

TABLE III: DATA OBTAINED FROM THE MORPHOLOGY OF TNTs.

Diameter	Thickness	Density	Surface Area
80 nm	2 μm	100 tubes/ μm^2	1909 mm^2

3.3 Raman Spectroscopy Evaluation

In order to detect the release of drug from the nanotubes, a valid method for capturing small concentrations of diluted drugs was needed. In a preliminary study gentamicin was used to evaluate whether or not the antibiotic showed a specific peak in the Raman spectra proportional to the concentration. The samples consisted of 15 μl droplet of diluted solution of gentamicin with different concentrations on a stainless steel substrate. Three different samples were evaluated: 10, 1 and 0.1 mg/ml of gentamicin dissolved in DPBS.

Figure 14 shows the Raman spectra for gentamicin, where it is evident that the antibiotic has a major characteristic peak at 992 cm^{-1} and a minor one at approximately 790 cm^{-1} , which are also the values reported in Zaleski et al. for gentamicin [53]. It is clear that the peak intensity is proportional to the concentration of antibiotic, but considering the high value of standard deviation and that there was one order of magnitude of difference among each of the samples, this detection method used with Raman spectroscopy cannot be considered valid to determine the precise concentration of drug in solution.

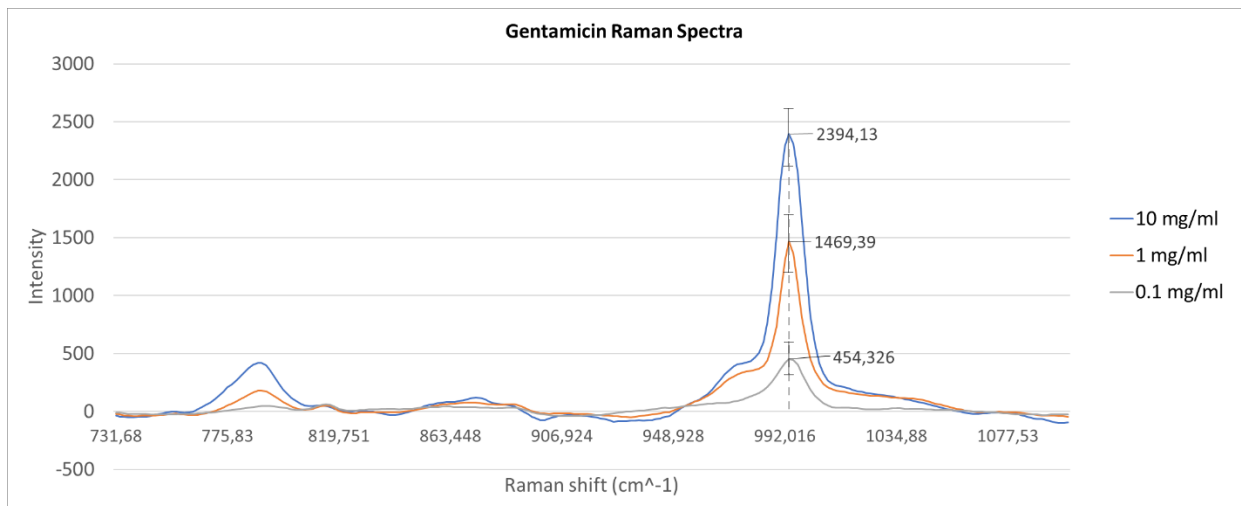


Figure 14: Gentamicin Raman spectra showing characteristic peaks for gentamicin, a major one at 992 cm^{-1} and a minor one at 790 cm^{-1} , for 3 different concentrations of the antibiotic: 10, 1 and 0.1 mg/ml diluted in DPBS. Considering there is one order of magnitude of difference among the samples, the data show results that are too scattered to consider Raman spectroscopy as a valid method to determine the precise concentration of drug in solution.

The reason for the highly scattered data lies in the diffusion mechanism of the droplet on the stainless steel substrate and its evaporation. As can be seen from Figure 15, once the droplet dries, single crystals of the antibiotic can be found spread unevenly on the surface. The fact that gentamicin crystals are not homogeneous on the surface interferes with an objective evaluation making it impossible to determine the actual drug concentration. Moreover, when a particle-laden droplet dries, it is subjected to the so called “coffee stain effect”, which causes the accumulation of particles along the perimeter of the stain. This mechanism introduces an even more inhomogeneous distribution of particles and confirms the inadequacy this detection method with Raman spectroscopy to determine the concentration not only for gentamicin, but every particle-laden solution.

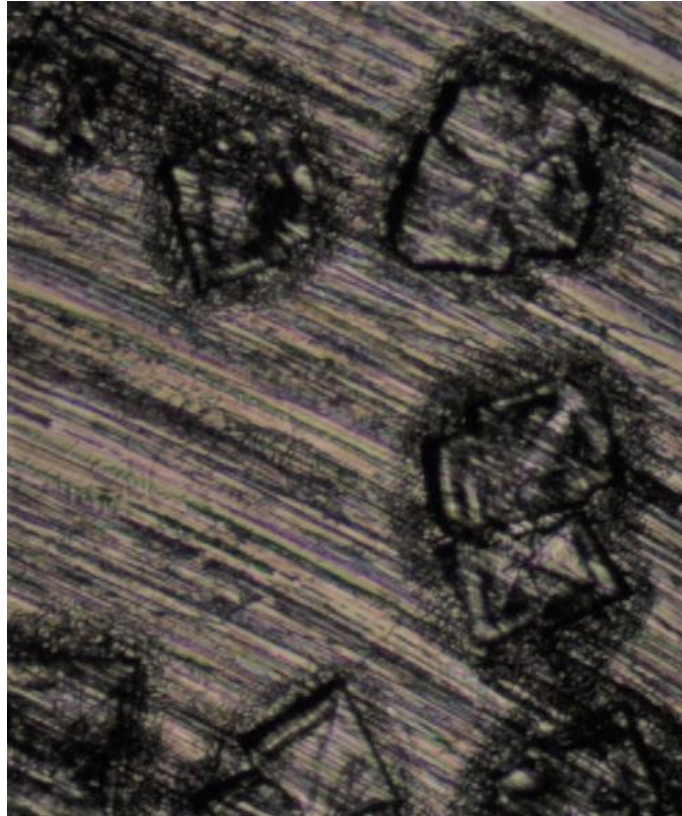


Figure 15: Close-up of gentamicin sample dried on stainless steel substrate taken with 50x objective. Single crystals spread unevenly on the surface making it a discriminating factor for an objective evaluation. The sample taken into consideration had a concentration of 10 $\mu\text{g/ml}$ of gentamicin diluted in DPBS.

3.4 Drug Release

When the idea of Raman spectroscopy was put aside, a new method for detecting drugs in solution was chosen. Literature suggested that the most accurate technique to determine the amount of substance diluted in solution, even at very low concentrations, was the use of UV-Vis spectroscopy [43], [44].

Instead of gentamicin, vancomycin was chosen because of its better efficacy against *S. aureus* since over time this bacterium developed resistance against gentamicin [54].

After the loading procedure, the K-wires were dipped in 400 μl of DPBS for the release of vancomycin and at different time steps, respectively 1, 5, 10, 30, 60 and 120 minutes, 300 μl out

of 400 were collected and pipetted into different wells of a 96-well plate. In the meantime, other wells of the same plate were filled with reference samples of known concentrations of vancomycin.

Figure 16 shows the calibration curve obtained from known concentration of vancomycin in order to associate the absorbance value returned by the UV-Vis spectrometer to the amount of antibiotic released in the solution. Absorbance is expected to have a linear relationship with the amount of antibiotic [47], which is confirmed by our experiment. The reference samples included DPBS only, 7.8, 15.63, 31.25, 62.5, 125, 250 and 500 $\mu\text{g/ml}$ of vancomycin diluted in DPBS.

The curve shows a very linear behavior for greater concentration of vancomycin, while for lower concentrations the UV-Vis spectrometer used in the experiment showed to have some detection limits as the curve appears to oscillate before stabilizing. The absorbance value returned by the spectrometer is relative for the specific system and it is not an absolute value valid for a set concentration of vancomycin. Every calculation for the release of vancomycin from the loaded K-wires was based on the values of absorbance from the reference samples.

For a future application, a more appropriate UV-Vis spectrometer with higher sensitivity should be adopted.

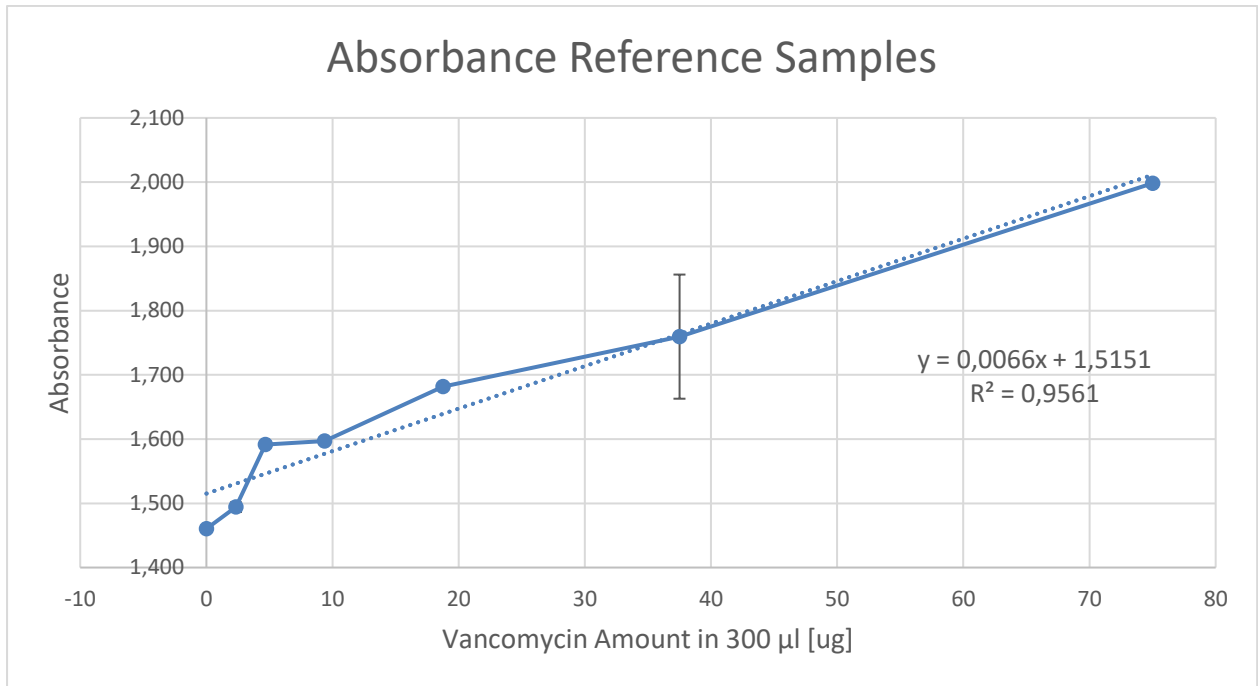


Figure 16: Calibration curve obtained from known concentrations of vancomycin diluted in DPBS in order to associate the value of absorbance returned by the UV-Vis spectrometer to the amount of vancomycin released in the solution. The samples chosen were DPBS only, 7.8, 15.63, 31.25, 62.5, 125, 250 and 500 µg/ml of vancomycin in DPBS.

The results of vancomycin release in 400 µl of DPBS are shown in

Figure 17. An initial burst of antibiotic is seen in the first minute of release, with an amount twice as high for the anodized wire with respect to the polished one. In the following time steps, the curve of the TNTs seems to have a constant release that reaches 90 µg of vancomycin released in 400 µl solution for a final concentration of 225 µg/ml after 2 hours.

Regarding the smooth Ti wires, we also see a big burst in the first minute, as we can expect, but the curve after 10 minutes is almost flat, showing that there is a very small release in the non-treated wires. Also, if we compare the two curves, we see that the slope is half as steep compared to the anodized wires, reaching a final release of about 50 µg of antibiotics after 2 hours.

The curves provide us with two different results: first, TNTs are able to host a much higher amount of molecules for a fast release in the first minutes, second, TNTs hold the antibiotic for a longer time inside the pores and release it in solution over time more than smooth Ti.

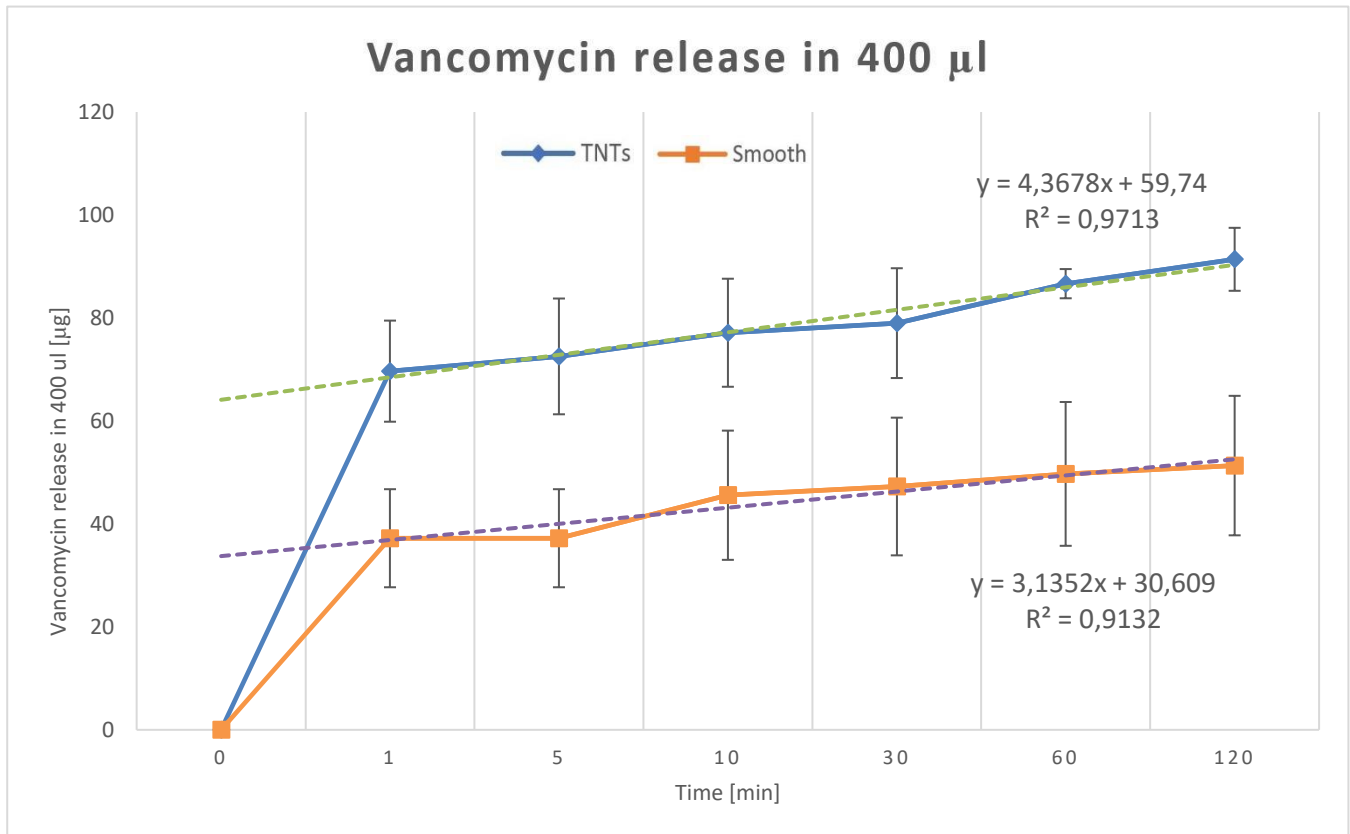


Figure 17: vancomycin released from K-wires in 400 µl of DPBS solution after different time steps. The initial burst from TNTs releases twice as much vancomycin in the first minute (blue) compared to smooth titanium (red). The TNTs curve also shows a steeper slope in the following time steps reaching a final release of vancomycin of about 90 µg compared to smooth titanium that releases about 50 µg after 2 hours.

3.5 Thickness Analysis

Now that we have data from the released antibiotic, we can double-check our initial hypothesis of the nanotubes thickness comparing the release from TNTs and smooth Ti. We assumed from Figure 13 a possible oxide thickness of 2 µm just looking at the length of the nanotubes. If we

suppose that we treated 20 mm of wire, which correspond to 37.98 mm² smooth surface area, a tube diameter of 80 nm, tube density of 100 pores/ μm^2 and consider that the vancomycin release after 2 hours was 50 μg from smooth surface and 90 μg from TNTs, we can calculate the thickness of nanotubes. Under the hypothesis that 100% of the nanotubes was completely loaded with antibiotic and the release of vancomycin is linearly proportional to the thickness, after doing some calculations, we obtain that the length of the nanotubes must be around 70 nm. This number is clearly in contrast with the depth shown in Figure 13. Hence, the only explanation must be that our hypothesis was wrong, that is, the nanotubes were not completely filled with vancomycin during the loading procedure, but only for a small percentage. This suggests that the loading procedure applied was not efficient enough and the full potential of the nanotubes was not exploited. The regular procedure for loading a solution into the nanotubes seems to be pipetting few droplets on the treated surface, drying under hood and repeating those steps several times [52], [55]–[58]. The same procedure cannot be used when using wires instead of flat surfaces, otherwise, there would be too much waste of solution. The loading procedure used in this work, which is dipping the wire in solution, drying it under hood and repeating the steps multiple times, must be improved for integrating more solution into the empty space of the nanotubes. A possible method could be increasing the number of times the wire is dipped and dried as well as increasing the dipping time. In this work, the loading procedure included 3 steps of dipping and drying, a dipping time of 10 minutes and a drying time of 30 minutes. It is recommended for future works to increase the dipping time and to gently shake the container to allow the solution to integrate better into the nanotubes for a longer and higher release in time.

In order to have a precise value of nanotubes thickness that is of great importance for understanding both the effect of the anodization on the morphology and the kinetics of drug release, a cross-section image at the SEM will be required.

CONCLUSIONS

This work proposed the anodization of titanium K-wires to form nanotubes on the oxide surface for drug release testing. It must be considered a preliminary work for future implantation in vivo to understand the kinetics of drugs inserted into the nanotubes. The morphology we obtained can be easily modified using different time and voltage parameters depending on the future application.

We successfully obtained 80 nm diameter nanotubes that host vancomycin solution for a local delivery as an antibacterial purpose.

The anodization increased the surface area of the K-wire by 50 times with respect to a smooth wire, increasing the adsorption of loaded vancomycin as well. The release tests showed a faster and higher release, about 80% more, of vancomycin from anodized wires compared to smooth titanium, confirming that implants with TNTs could be used as a possible vehicle to release drugs locally. However, the increase in the release does not match the increase in surface area, suggesting that the nanotubes were not filled completely and therefore, a more efficient loading procedure must be proposed.

This procedure remains a valid option for implantation in vivo for the enhanced osseointegration and drug release properties offered by TNTs.

FUTURE WORK

TNTs provide a better loading of vancomycin as well as a faster and longer release over time, even if this work presents limitations that can be overcome with adjustments in future works.

As previously cited, it is important to perform cross-section images of the sample at the SEM in order to define the thickness of TNTs layer on the surface. This is helpful in understanding both the morphology related to the anodization and the release kinetics of drugs.

In alternative, in order to measure the exact value of the surface area, the Brunauer, Emmett and Teller (BET) technique can be used [59]. BET exploits a gas, usually nitrogen, which adsorbs on the entire surface of the sample. The volume of the adsorbed gas corresponds to a precise value of surface area. This technique would also be very useful to understand if some remains of the electrolyte were kept into the nanotubes even after the process. To prevent that, before the drug loading procedure, it is recommended to put the anodized wire under vacuum to eliminate any possible leftover of the reaction.

Another important fact is to improve the loading procedure since it was hypothesized it is the cause for the relatively small difference in the release of vancomycin between anodized and smooth wires. An increase in dipping time is required in order to allow the solution to flow into the nanotubes. This step must be performed multiple times.

The morphology of TNTs can be optimized using different parameters depending on the releasing substance. The voltage is known to be directly proportional to the diameter dimension, while the anodization time is proportional to the length of the nanotube. For a higher and faster release, it is recommended to obtain larger pores, while for a longer effect in time, a wire with a higher surface area and smaller tubes is more appropriate.

In order to obtain an ordered nanotubes morphology, it is important to have a well-polished surface prior the anodization. The nanotubes grow perpendicular on the surface and if it is not perfectly smooth, we will not obtain a highly ordered structure, as we can see from Figure 10. In a future work, electrochemical polishing is required for building the nanostructure on a smoother substrate.

The drug release procedure must be optimized as well. We detected some sensitivity issues, which could be addressed to multiple reasons. The most probable one is the use of a plastic made plate that interfered with the actual values of absorbance, so for a future application, it is recommended to use a UV-transparent plate. If the sensitivity issue persists, another spectrometer must be used. The UV-Vis spectrometer must be appropriate for the task and have a sensitivity high enough to detect with small precision concentrations of vancomycin in solution.

Moreover, different drugs can be mixed in the same implant in order to treat different threats simultaneously.

CITED LITERATURE

- [1] C. N. Elias, J. H. C. Lima, R. Valiev, and M. A. Meyers, “Biomedical applications of titanium and its alloys Biological Materials Science 46-49,” *Biol. Mater. Sci.*, no. March, pp. 1–4, 2008.
- [2] X. Liu, P. K. Chu, and C. Ding, “Surface modification of titanium, titanium alloys, and related materials for biomedical applications,” *Mater. Sci. Eng. R Reports*, vol. 47, no. 3–4, pp. 49–121, 2004, doi: 10.1016/j.mser.2004.11.001.
- [3] Z. Fei Yin, L. Wu, H. Gui Yang, and Y. Hua Su, “Recent progress in biomedical applications of titanium dioxide,” *Phys. Chem. Chem. Phys.*, vol. 15, no. 14, pp. 4844–4858, 2013, doi: 10.1039/c3cp43938k.
- [4] A. Barfeie, J. Wilson, and J. Rees, “Implant surface characteristics and their effect on osseointegration,” *Br. Dent. J.*, vol. 218, no. 5, 2015, doi: 10.1038/sj.bdj.2015.171.
- [5] M. Windler and R. Klabunde, “Titanium for Hip and Knee Prostheses,” pp. 703–746, 2001, doi: 10.1007/978-3-642-56486-4_21.
- [6] M. Sloan, A. Premkumar, and N. P. Sheth, “Projected Volume of Primary Total Joint Arthroplasty,” pp. 1455–1460, 2018.
- [7] H. M. Kremers *et al.*, “Prevalence of Total Hip and Knee Replacement in the United States,” pp. 1386–1397, 2015.
- [8] “Orthopedic Implants Market Size, Share & Industry Analysis, By Products (Joint Reconstruction, Spinal Implants, Trauma Implants, Dental Implants, Orthobiologics and Others) End-Users (Hospitals, Orthopedic Clinics, Ambulatory Surgical Centers) and Regiona.” [Online]. Available: <https://www.fortunebusinessinsights.com/industry-reports/orthopedic-implants-market-101659>.

- [9] G. Li, Q. M. Zhao, H. L. Yang, and L. Cheng, "Antibacterial and microstructure properties of titanium surfaces modified with Ag-incorporated nanotube arrays," *Mater. Res.*, vol. 19, no. 3, pp. 735–740, 2016, doi: 10.1590/1980-5373-MR-2015-0534.
- [10] B. Li and T. Fintan, *Racing for the Surface*. .
- [11] W. Feng *et al.*, "Controlled release behaviour and antibacterial effects of antibiotic-loaded titania nanotubes," *Mater. Sci. Eng. C*, vol. 62, pp. 105–112, 2016, doi: 10.1016/j.msec.2016.01.046.
- [12] C. Jacqueline and J. Caillon, "Impact of bacterial biofilm on the treatment of prosthetic joint infections," *J. Antimicrob. Chemother.*, vol. 69, no. SUPPL1, pp. 37–40, 2014, doi: 10.1093/jac/dku254.
- [13] G. Koch, "Medicinal Chemistry," *Chimia (Aarau)*., vol. 71, no. 10, p. 643, 2017, doi: 10.1021/ie50495a015.
- [14] Z. Peng *et al.*, "Dual effects and mechanism of TiO₂ nanotube arrays in reducing bacterial colonization and enhancing C3H10T1/2 cell adhesion," *Int. J. Nanomedicine*, vol. 8, pp. 3093–3105, 2013, doi: 10.2147/IJN.S48084.
- [15] S. Francisco and S. Francisco, "AFTER TOTAL H I P ARTHROPLASTY," pp. 1746–1752, 2005.
- [16] K. L. Ong, S. M. Kurtz, E. Lau, K. J. Bozic, D. J. Berry, and J. Parvizi, "Prosthetic Joint Infection Risk After Total Hip Arthroplasty in the Medicare Population," *J. Arthroplasty*, vol. 24, no. 6, pp. 105–109, 2009, doi: 10.1016/j.arth.2009.04.027.
- [17] S. M. Kurtz, E. Lau, H. Watson, J. K. Schmier, and J. Parvizi, "Economic Burden of Periprosthetic Joint Infection in the United States," *J. Arthroplasty*, vol. 27, no. 8, pp. 61–65.e1, 2012, doi: 10.1016/j.arth.2012.02.022.

- [18] N. D. Friedman, B. Health, K. Kirkland, W. J. Richardson, and D. J. Sexton, “The Impact of Surgical - Site Infections Following Orthopedic Surgery at a Community Hospital and a University Hospital: Adverse Quality of Life , F O L L O W I N G O R T H O P E D I C S U R G E R Y A T A C O M M U N I T Y H O S P I T A L A N D A U N I V E R S I T Y H O S P I T A L : A D V E R S E Q U A L I T Y O,” no. May, 2014, doi: 10.1086/502033.
- [19] S. M. Kurtz, K. L. Ong, E. L. Ms, K. J. Bozic, and D. Berry, “Prosthetic Joint Infection Risk after TKA in the Medicare Population,” pp. 52–56, 2010, doi: 10.1007/s11999-009-1013-5.
- [20] B. H. Kapadia, S. Banerjee, J. J. Cherian, K. J. Bozic, and M. A. Mont, “The Economic Impact of Periprosthetic Infections After Total Hip Arthroplasty at a Specialized Tertiary-Care Center,” *J. Arthroplasty*, vol. 31, no. 7, pp. 1422–1426, 2016, doi: 10.1016/j.arth.2016.01.021.
- [21] B. H. Kapadia, M. J. Mcelroy, K. Issa, A. J. Johnson, K. J. Bozic, and M. A. Mont, “The Economic Impact of Periprosthetic Infections Following Total Knee Arthroplasty at a Specialized Tertiary-Care Center,” *J. Arthroplasty*, vol. 29, no. 5, pp. 929–932, 2014, doi: 10.1016/j.arth.2013.09.017.
- [22] Y. Li *et al.*, “Enhanced antibacterial properties of orthopedic implants by titanium nanotube surface modification: A review of current techniques,” *Int. J. Nanomedicine*, vol. 14, pp. 7217–7236, 2019, doi: 10.2147/IJN.S216175.
- [23] V. S. Saji, H. C. Choe, and K. W. K. Yeung, “Nanotechnology in biomedical applications: A review,” *Int. J. Nano Biomater.*, vol. 3, no. 2, pp. 119–139, 2010, doi: 10.1504/IJNBM.2010.037801.
- [24] K. C. Popat, M. Eltgroth, T. J. LaTempa, C. A. Grimes, and T. A. Desai, “Titania nanotubes: A novel platform for drug-eluting coatings for medical implants?,” *Small*, vol. 3, no. 11,

- pp. 1878–1881, 2007, doi: 10.1002/sml.200700412.
- [25] M. S. Alhoshan, A. A. Baqais, M. I. Al-Hazza, and A. M. Al-Mayouf, “Heat treatment and electrochemical activation of titanium oxide nanotubes: The effect of hydrogen doping on electrochemical behavior,” *Electrochim. Acta*, vol. 62, pp. 390–395, 2012, doi: 10.1016/j.electacta.2011.12.048.
- [26] “Development of Titanium Surgery Implants for Improving Osseointegration Through Formation of a Titanium Nanotube Layer,” vol. 9, pp. 32–45, 2014.
- [27] L. M. Bjursten, L. Rasmusson, S. Oh, G. C. Smith, K. S. Brammer, and S. Jin, “Titanium dioxide nanotubes enhance bone bonding in vivo,” *J. Biomed. Mater. Res. - Part A*, vol. 92, no. 3, pp. 1218–1224, 2010, doi: 10.1002/jbm.a.32463.
- [28] X. Zhang, Z. Zhang, G. Shen, and J. Zhao, “Enhanced osteogenic activity and anti-inflammatory properties of Lenti-BMP-2-loaded TiO₂ nanotube layers fabricated by lyophilization following trehalose addition,” *Int. J. Nanomedicine*, vol. 11, pp. 429–439, 2016, doi: 10.2147/IJN.S93177.
- [29] “Anodizing.” [Online]. Available: <https://en.wikipedia.org/wiki/Anodizing>.
- [30] J. M. Macak *et al.*, “TiO₂ nanotubes: Self-organized electrochemical formation, properties and applications,” *Curr. Opin. Solid State Mater. Sci.*, vol. 11, no. 1–2, pp. 3–18, 2007, doi: 10.1016/j.cossms.2007.08.004.
- [31] P. Roy, S. Berger, and P. Schmuki, “TiO₂ nanotubes: Synthesis and applications,” *Angew. Chemie - Int. Ed.*, vol. 50, no. 13, pp. 2904–2939, 2011, doi: 10.1002/anie.201001374.
- [32] N. Ohtsu, T. Kozuka, M. Hirano, and H. Arai, “Electrolyte effects on the surface chemistry and cellular response of anodized titanium,” *Appl. Surf. Sci.*, vol. 349, pp. 911–915, 2015, doi: 10.1016/j.apsusc.2015.05.046.

- [33] S. Minagar, C. C. Berndt, J. Wang, E. Ivanova, and C. Wen, "A review of the application of anodization for the fabrication of nanotubes on metal implant surfaces," *Acta Biomater.*, vol. 8, no. 8, pp. 2875–2888, 2012, doi: 10.1016/j.actbio.2012.04.005.
- [34] J. Kim *et al.*, "Effects of NH₄F and distilled water on structure of pores in TiO₂ nanotube arrays," *Sci. Rep.*, vol. 8, no. 1, pp. 4–11, 2018, doi: 10.1038/s41598-018-30668-3.
- [35] D. Regonini, C. R. Bowen, A. Jaroenworarluck, and R. Stevens, "A review of growth mechanism, structure and crystallinity of anodized TiO₂ nanotubes," *Mater. Sci. Eng. R Reports*, vol. 74, no. 12, pp. 377–406, 2013, doi: 10.1016/j.mser.2013.10.001.
- [36] S. Url, R. Society, P. Sciences, and T. R. Society, "The Morphology and Mechanism of Formation of Porous Anodic Films on Aluminium J . P . O ' Sullivan ; G . C . Wood," vol. 317, no. 1531, pp. 511–543, 1970.
- [37] D. D. Macdonald, "On the Formation of Voids in Anodic Oxide Films on Aluminum," *J. Electrochem. Soc.*, vol. 140, no. 3, p. L27, 1993, doi: 10.1149/1.2056179.
- [38] T. Sawitowski, "Neue Nanokomposite," *Diss. Univ. Ess.*, pp. 54–85, 1999.
- [39] S. Wu, S. Wang, W. Liu, X. Yu, G. Wang, and Z. Chang, "Surface & Coatings Technology Microstructure and properties of TiO₂ nanotube coatings on bone plate surface fabrication by anodic oxidation," vol. 374, no. June, pp. 362–373, 2019, doi: 10.1016/j.surfcoat.2019.06.019.
- [40] J. Wan, X. Yan, J. Ding, M. Wang, and K. Hu, "Self-organized highly ordered TiO₂ nanotubes in organic aqueous system," *Mater. Charact.*, vol. 60, no. 12, pp. 1534–1540, 2009, doi: 10.1016/j.matchar.2009.09.002.
- [41] "Ammonium Fluoride | Pubchem." [Online]. Available: <https://pubchem.ncbi.nlm.nih.gov/compound/Ammonium-fluoride#section=Reactivity->

Profile.

- [42] Sigma, "Product information Gentamicin sulfate salt," *Laboratory Medicine*. pp. 1986–1986, 1986.
- [43] E. K. Nickerson *et al.*, "Staphylococcus aureus bacteraemia in a tropical setting: Patient outcome and impact of antibiotic resistance," *PLoS One*, vol. 4, no. 1, 2009, doi: 10.1371/journal.pone.0004308.
- [44] C. Rayner and W. J. Munckhof, "Antibiotics currently used in the treatment of infections caused by Staphylococcus aureus," *Intern. Med. J.*, vol. 35, no. SUPPL. 2, 2005, doi: 10.1111/j.1444-0903.2005.00976.x.
- [45] J. Martínez-moreno, V. Merino, A. Nácher, J. L. Rodrigo, M. Climente, and M. Merino-sanjuán, "Antibiotic-loaded Bone Cement as Prophylaxis in Total Joint Replacement Evidence of Effectiveness and Safety," no. February, pp. 331–341, 2017, doi: 10.1111/os.12351.
- [46] "UV-Vis Spectroscopy." [Online]. Available: https://en.wikipedia.org/wiki/Ultraviolet-visible_spectroscopy.
- [47] M. H. Tariq, H. Naureen, N. Abbas, and M. Akhlaq, "Development and validation of a method for the analysis of vancomycin in human serum using ultracentrifuge protein precipitation and UV spectroscopy," *Lat. Am. J. Pharm.*, vol. 34, no. 8, pp. 1489–1496, 2015, doi: 10.4172/2155-9872.1000239.
- [48] H. W. Kim, J. C. Knowles, and H. E. Kim, "Hydroxyapatite porous scaffold engineered with biological polymer hybrid coating for antibiotic Vancomycin release," *J. Mater. Sci. Mater. Med.*, vol. 16, no. 3, pp. 189–195, 2005, doi: 10.1007/s10856-005-6679-y.
- [49] B. Ercan, E. Taylor, and E. Alpaslan, "Diameter of titanium nanotubes influences anti-

- bacterial efficacy,” no. May 2014, 2011, doi: 10.1088/0957-4484/22/29/295102.
- [50] K. C. Popat, M. Eltgroth, T. J. LaTempa, C. A. Grimes, and T. A. Desai, “Decreased *Staphylococcus epidermis* adhesion and increased osteoblast functionality on antibiotic-loaded titania nanotubes,” *Biomaterials*, vol. 28, no. 32, pp. 4880–4888, 2007, doi: 10.1016/j.biomaterials.2007.07.037.
- [51] G. A. Crawford, N. Chawla, K. Das, S. Bose, and A. Bandyopadhyay, “Microstructure and deformation behavior of biocompatible TiO₂ nanotubes on titanium substrate,” *Acta Biomater.*, vol. 3, no. 3 SPEC. ISS., pp. 359–367, 2007, doi: 10.1016/j.actbio.2006.08.004.
- [52] A. Hamlekhan *et al.*, “Fabrication of drug eluting implants: Study of drug release mechanism from titanium dioxide nanotubes,” *J. Phys. D. Appl. Phys.*, vol. 48, no. 27, 2015, doi: 10.1088/0022-3727/48/27/275401.
- [53] S. Zaleski, K. A. Clark, M. M. Smith, J. Y. Eilert, M. Doty, and R. P. Van Duyne, “Identification and Quantification of Intravenous Therapy Drugs Using Normal Raman Spectroscopy and Electrochemical Surface-Enhanced Raman Spectroscopy,” *Anal. Chem.*, vol. 89, no. 4, pp. 2497–2504, 2017, doi: 10.1021/acs.analchem.6b04636.
- [54] J. E. Dowding, “Mechanisms of Gentamicin Resistance in *Staphylococcus aureus*,” vol. 11, no. 1, pp. 47–50, 1977.
- [55] W. T. Lin *et al.*, “Inhibited bacterial biofilm formation and improved osteogenic activity on gentamicin-loaded titania nanotubes with various diameters,” *Int. J. Nanomedicine*, vol. 9, no. 1, pp. 1215–1230, 2014, doi: 10.2147/IJN.S57875.
- [56] Y. Yang *et al.*, “In vivo evaluation of the anti-infection potential of gentamicin-loaded nanotubes on titania implants,” *Int. J. Nanomedicine*, vol. 11, pp. 2223–2234, 2016, doi: 10.2147/IJN.S102752.

- [57] H. Z. Zhang *et al.*, “Improved antibacterial activity and biocompatibility on vancomycin-loaded TiO₂ nanotubes: In vivo and in vitro studies,” *Int. J. Nanomedicine*, vol. 8, pp. 4379–4389, 2013, doi: 10.2147/IJN.S53221.
- [58] K. Gulati, M. S. Aw, and D. Losic, “Drug-eluting Ti wires with titania nanotube arrays for bone fixation and reduced bone infection,” *Nanoscale Res. Lett.*, vol. 6, no. 1, pp. 1–6, 2011, doi: 10.1186/1556-276X-6-571.
- [59] “BET.” [Online]. Available: <https://particle.dk/methods-analytical-laboratory/surface-area-bet-2/>.

VITA

NAME: Lorenzo Girotto

EDUCATION: Scientific High School Diploma (2010-2015), Liceo Giacomo Leopardi, Milan, Italy

Bachelor of Science in Biomedical Engineering (2015-2018), Politecnico di Milano, Milan, Italy

Master of Science in Biomedical Engineering (ongoing since 2018), Politecnico di Milano, Milan, Italy

Master of Science in Bioengineering (ongoing since 2019), University of Illinois at Chicago, Chicago, USA

WORK EXPERIENCE: Graduate Student Researcher for Rush University Medical Center, Department of Orthopedics, Chicago, IL, USA